Alluvial fan aggradation/incision history of the eastern Tibetan plateau margin and implications for debris flow/debris-charged flood hazard

Yajun Li[1,2*], Simon Armitage[1,3], Thomas Stevens[4], Xingmin Meng[2]

1 Center for Quaternary Research, Department of Geography, Royal Holloway University of London, Egham, Surrey, TW20 0EX, United Kingdom

2 Key Laboratory of Western China's Environmental Systems (Ministry of Education), College of Earth and Environmental Sciences, Lanzhou University, Lanzhou, 73000, China.

3 SFF Centre for Early Sapiens Behaviour (SapienCE), University of Bergen, Post Box 7805, 5020, Bergen, Norway

4 Department of Earth Sciences, Villavägan 16, Uppsala University, 75236 Uppsala, Sweden

Abstract

This paper reconstructs the Quaternary aggradation and incision history of a debris flow/debris-charged flood-affected valley in order to detect the impact of climate on alluvial fan dynamics. We used optically stimulated luminescence (OSL) dating of quartz to determine the ages of alluvial fan terraces. Comparison between the aggradation and incision history and regional climatic records

suggests that aggradation occurred in cold and/or dry climates, whereas incision is a feature of warm and wet climates. Cold climates lead to enhanced frost shattering, and dry climates cause deteriorated vegetation. Both effects caused surplus sediment, which was transported by infrequent flood discharges to form alluvial fan/terrace deposits. Incision during wet and warm climates is due to increased vegetation cover and an increase in the frequency of flood discharges. This relationship between climate and valley evolution is applied to assess future changes in the present active channel by considering recent climatic records. The results show that the valley channel is expected to experience net incision if the average temperature continues increasing while precipitation maintains at a constant level.

Key words: Alluvial fan, aggradation and incision, Tibetan Plateau, OSL dating

1. Introduction

The eastern margin of the Tibetan Plateau is characterized by large rivers incising into the uplifted topography resulting from the continued convergence between the Indian and Eurasian plates (Clark and Royden, 2000; Kirby et al., 2002; Ouimet et al., 2007). Alluvial sediments, which are sourced from tributary valleys, are deposited on the valley floors of these large rivers, forming tributary-junction alluvial fans (Harvey, 1997, 2011; Al-Farraj and Harvey, 2000, 2005; Stokes and Mather, 2015). These types of alluvial fans have smaller extensional areas than those developed in mountain-front settings (Sohn et al., 2007; Spelz

et al., 2008; Kar et al., 2014; Harvey et al., 2016), whilst they usually develop multiple fan levels representing alternations between aggradation and incision (Harvey and Renwick, 1987; Al-Farraj and Harvey, 2000; Harvey, 2002; Juyal et al., 2010).

Knowledge of the factors causing changes of regime between aggradation and incision has been a key question in alluvial fan research (Harvey, 2012; Owen et al., 2014). Understanding the regime is crucial in regulating fan-building processes such as debris flows or floods for hazard mitigation (Jakob, 2005; Welsh and Davies, 2011; Santangelo et al., 2012). This need is particularly urgent in the eastern margin of the Tibetan Plateau, where a proportion of the population lives on the alluvial fans (Tang et al., 2011; Zhang et al., 2011; Xiong et al., 2016). Among the factors that influence fan development (e.g., tectonism, climate and base level), climate has been regarded as a dominant factor in millennial timescales across the world (Ritter et al., 1995; McDonald et al., 2003; Pope and Wilkinson, 2005; Suresh et al., 2007; Kar et al., 2014; Owen et al., 2014). This paper aims to understand the relationship between fan dynamics and climate in a tributary valley of the Bailong River, which is one of the main rivers connecting the Tibetan Plateau and the Sichuan Basin.

Detailed mapping and borehole drilling highlight four stages of

62 aggradation/incision during the evolution of alluvial fans in the valley. Here, we
63 produce a chronology for the aggradation and incision periods using optically
64 stimulated luminescence (OSL) dating of quartz derived from terrace and
65 borehole sediments. The aggradation and incision periods are then compared
66 with well-dated regional climatic records to examine how alluvial processes
67 respond to climatic changes. Finally, the past relationships between climate and
68 valley evolution are used to infer future debris flow/debris-charged flood hazards
69 in the valley, representing a new approach to understanding long-term debris
70 flow/debris-charged flood hazards.

71 **2. Research contexts**

72 *2.1. Study area*

73 The Bailong River is a primary tributary of the Yangtze River. It originates on the
74 Tibetan Plateau at an elevation of ~ 6000 m and flows southeast through three
75 counties, Zhouqu, Wudu and Wen, of Gansu Province (Fig. 1). The middle
76 section of the Bailong River (i.e., between Zhouqu and Wudu) (Fig. 1), is an area
77 with locally high population density. The county centers of Zhouqu and Wudu,
78 and various other town centers, are situated on the alluvial fans or fluvial terraces
79 of this section of the river. Geologically, this section of the river has developed in
80 an anticline system (Li, 1994) that folded the region between the Silurian and
81 Permian. The anticline hinge was eroded, forming relatively low-relief, low-

elevation hillslopes and river valleys (Zhang et al., 2011), while the anticline limbs formed high-relief, high-elevation hillslopes that became the headwaters of tributary valleys feeding the Bailong River.

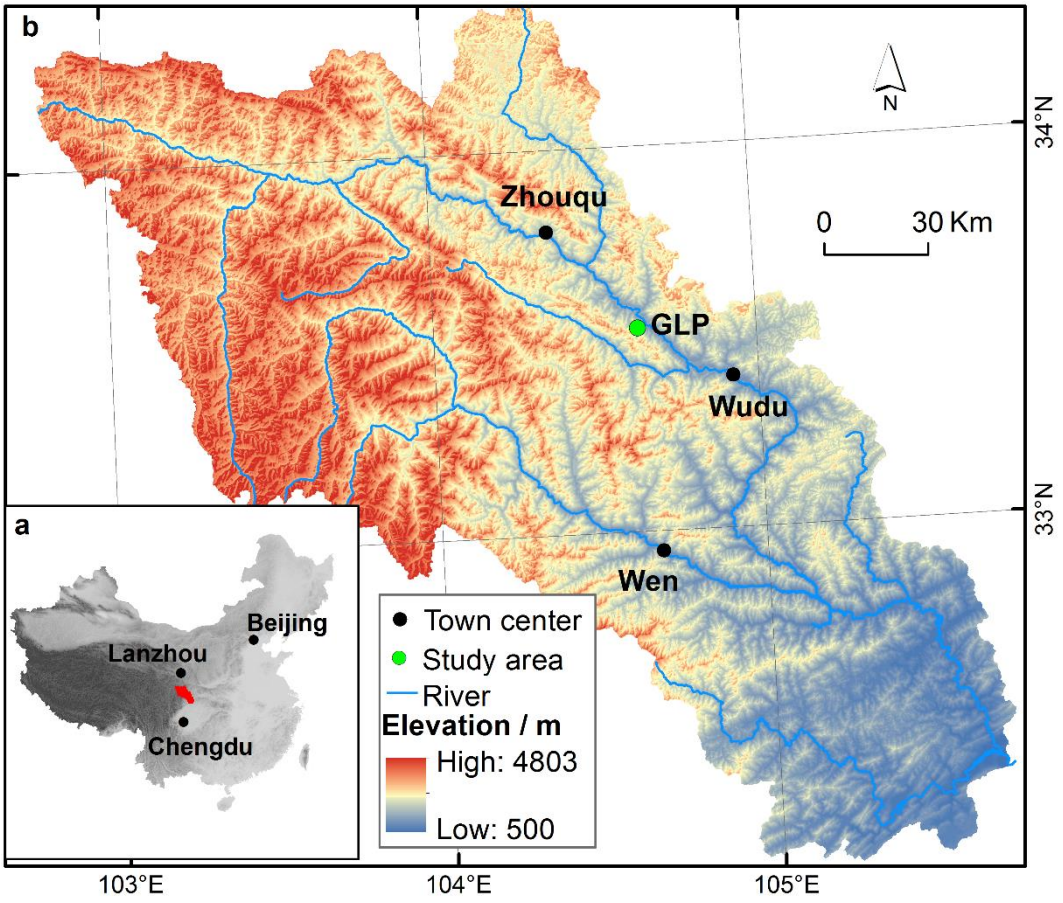

Fig. 1. Location of the Bailong River and the GLP valley. (a). Location of the watershed (the area shaded in red) within China. (b). DEM of the Bailong River watershed and the location of the GLP valley. The background image is a 30-m resolution ASTER DEM. Zhouqu, Wudu and Wen are the three important county centers along the Bailong River.

The Goulinping (GLP) River (N 33˚32′24″, E 104˚ 39′13″), with a watershed area

of ~ 20 km^2 and a relief of 1897 m, is located in the middle section of the Bailong River (Fig. 2). It is sourced from a high-relief limestone area and subsequently passes through a low-relief phyllite area before finally entering the Bailong River (Fig. 3). To demonstrate the representativeness of the GLP River in the middle section of the Bailong River, three key geomorphic parameters, drainage area (A), hypsometric integrals (HI) and relief of the tributary valleys were calculated using the spatial analyst tools in ArcGIS 10.2 (Fig. 2). Tributary valleys in the middle section of the Bailong can be grouped into three categories based on their drainage areas: small-sized valleys ($A < 10$ km^2), intermediate-sized valleys ($10 \leq A \leq 100$ km^2) and large-sized valleys ($A > 100$ km^2) (Fig. 2b). Figure 2 demonstrates that the intermediate-sized tributary valleys account for a primary proportion of the middle section of the Bailong and generally developed from relatively high-elevation (> 2500 m) areas. These intermediate-sized valleys have HI values between 0.41 and 0.60 (Fig 2c), and relief between 1645 and 2405 m (Fig. 2d). The GLP valley (intermediate-sized) has a HI value of 0.47 and a relief of 1897 m, both of which fall in the range of the HI and relief values for the intermediate-sized valleys, making it representative of many intermediate-sized tributary valleys in the middle section of the Bailong River.

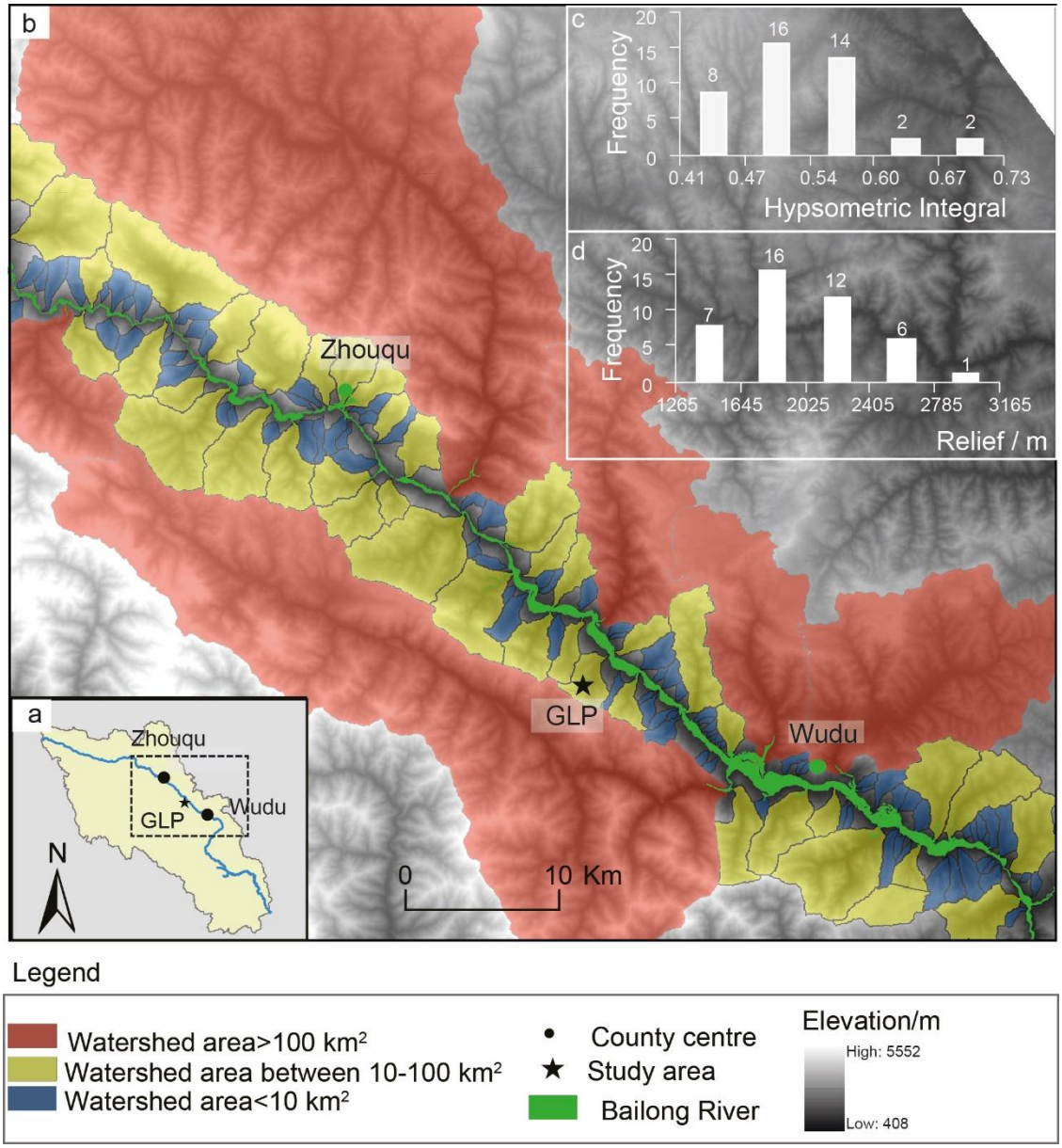

111

112 Fig. 2. Tributary valleys in the middle section of the Bailong River. (a). The
113 watershed boundary of the middle section of the Bailong River (dashed box). (b).
114 Tributary valleys classified by watershed area. The star symbol denotes the
115 location of the GLP valley. (c). The frequency of the hypsometric integrals of the
116 intermediate-sized valleys. (d). The frequency of the relief of the intermediate-
117 sized valleys.

Climate in the study area is controlled by the Asian monsoon system, which is characterized by warm and humid summers and dry and cold winters (Railsback et al., 2014). The area receives an annual precipitation of 487.2 mm, 75 to 85% of which falls between May and September. The average minimum and maximum temperatures are −14 °C to 3 °C in January, and 11 °C to 27 °C in July (Johnson et al., 2006).

2.2 Alluvial fan/terrace settings

Four levels of alluvial fans/terraces (denoted as F1, F2, F3 and F4 from the lowest to the highest elevation) are identified based on field investigation (Fig. 3). These sedimentary bodies are characterized by alluvial fans at the valley mouth and alluvial terraces upstream. These alluvial terraces sourced from the limestone headwaters have fed the alluvial fans at the valley mouth. The F3 and F4 alluvial fans/terraces are distributed across the phyllite valley, while the F1 and F2 alluvial fans/terraces are only present close to the phyllite valley mouth (Fig. 3).

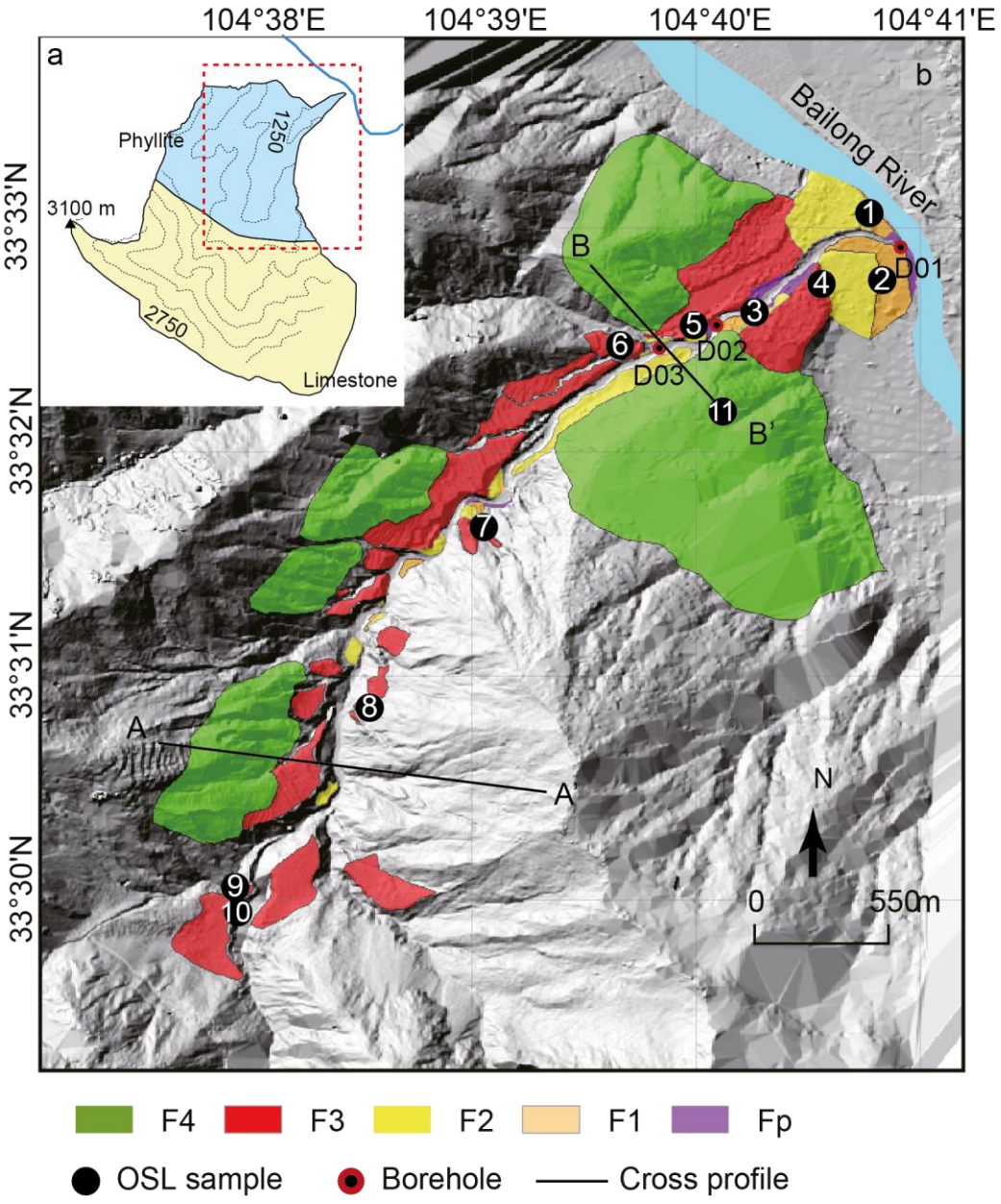

135

136 Fig. 3. Geomorphic setting of the GLP valley. (a). The watershed of the GLP
137 valley. The contour interval is 250 m with the highest point (3100 m) shown by a
138 filled triangle. The dashed red box delineates the phyllite area, which is shown
139 in Fig. 3b. (b). The alluvial fan/terrace distribution and locations of boreholes and
140 OSL samples. The two cross-valley transects (A-A' and B-B') are displayed in
141 Fig. 6. The background image is a hill-shade image of the GLP valley. The

numbered black circles indicate the locations of the OSL samples, which are shown in Fig. 7.

The sedimentology of these alluvial fans/terraces was described using four sedimentary logs for each fan/terrace level (Fig. 4). These alluvial terraces/fans are mainly formed by debris flows/debris-charged floods. The facies representing debris flow deposition are clast-supported massive pebble to cobble gravels (Gcm), clast-supported inversely graded pebble to cobble gravels (Gci) and matrix-supported massive pebble to cobble gravels (Gmm). The facies representing debris-charged floods are crudely-bedded pebble to cobble gravels (Gh). There are some thin sedimentary bodies that developed well-bedded gravels with upward fining trends (Gh'), indicating deposition by small streamfloods. All these facies are characterized by sub-angular to sub-rounded limestone-dominated gravels, indicating that they were sourced from the limestone headwaters. Generally, the debris flow sediments are non-erosive, forming net aggradation, though occasionally erosive bases were identified (Fig 4, F2). In contrast, the debris-charged flood sediments have erosive concave scars at their base (Fig. 4, F3), indicating some early stage erosion during a flooding event.

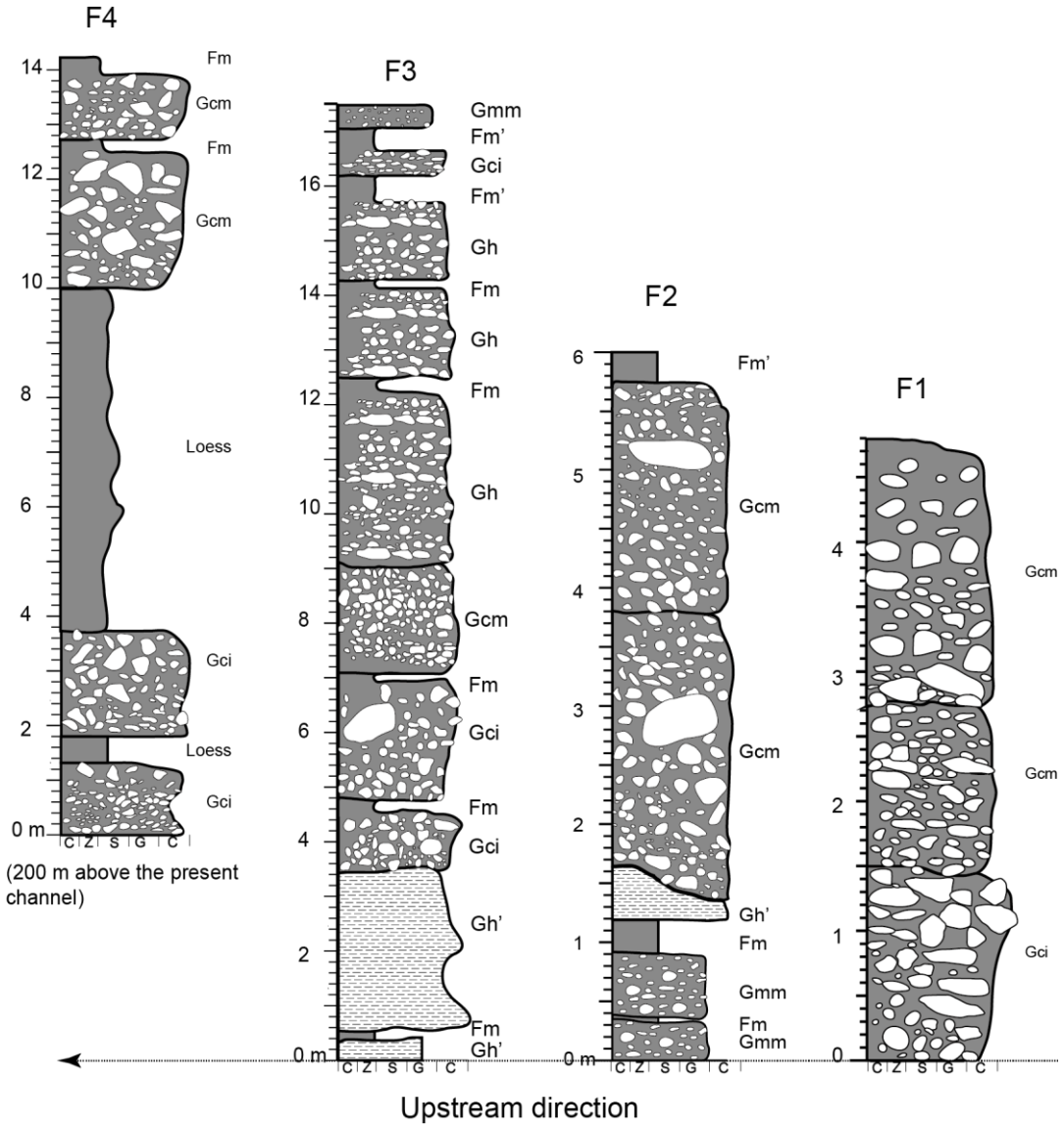

Fig. 4. Sedimentary logs for different alluvial fans/terraces. The horizontal axis represents the channel floor (directed upstream). The F4 profile is a portion of the upper part of an F4 terrace.

Intercalated between these primary facies are some thin layers of pale yellowish orange (10YR 8/6) silt that shows weak stratification and contains small granules (Fm). The pale yellowish orange color suggests that these silty sediments are

loessic materials because localized bedrock (phyllite) eroded fine materials are generally gray in color. The weak horizontal stratification and the incorporation of granules suggest the operation of fluvial processes. Collectively, this type of sediment was likely deposited by slow and continuous overbank flows that transported hillslope-eroded loess. The abundance of loessic fines suggests a relatively unstable hillslope surface covered by aeolian loess. Overlying the F2 and F3 alluvial fans/terraces are relatively thick (> 40 cm) layers of yellowish brown silt that contains plant roots and soil nodules (Fm'). These layers are interpreted as paleosols. On top of the F4 sediments are thick (>10 m) relatively homogeneous yellowish brown silt indicating aeolian deposition undisturbed by alluvial processes. Typical photographs showing the characteristics of different facies are provided in Supplementary Materials (SM), Fig. S1.

Three boreholes (i.e., D01, D02 and D03) were drilled into the present valley floor at the downstream section of the valley (Fig. 3) using a rotary drilling machine (SM, Fig. S2). The boreholes reached a depth of 62 m (D01), 45 m (D02) and 52 m (D03) beneath the present channel (Fig. 5). Simplified sedimentary logs of the three boreholes are provided in SM, Fig. S4.

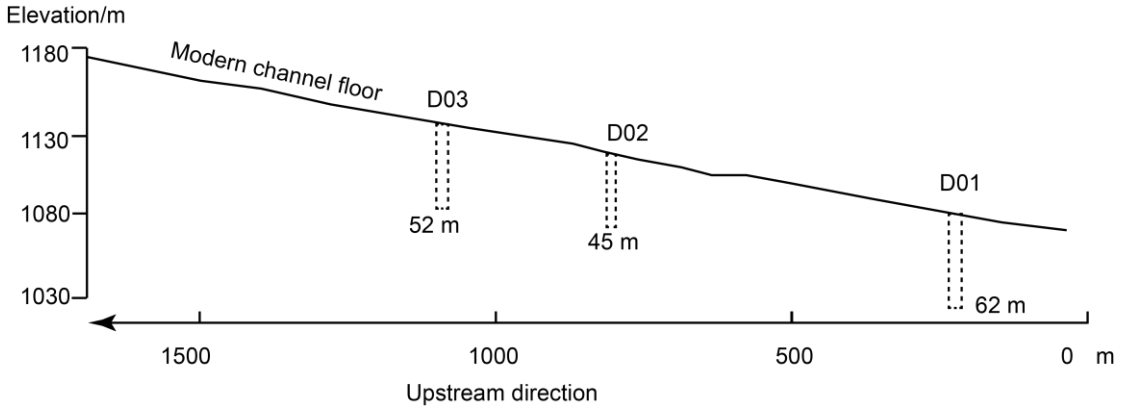

Fig. 5. Depth of the three boreholes.

2.3. Phases of alluvial fan/terrace aggradation and incision

Observations of these four levels of alluvial fans/terraces, together with the three boreholes (Fig. 5), highlight four stages of aggradation/incision: (1) the first aggradation period (S1) that formed the F4 alluvial fans, (2) the subsequent incision period (S2) during which the F4 alluvial fans and the underlying phyllite bedrock were incised through, (3) the second aggradation period (S3) that formed the F3 alluvial fans, and (4) the incision period (S4) that featured dissection of the F3 alluvial terraces/fans and two small aggradation periods of the F1 and F2 alluvial fans. The depth of incision/aggradation is illustrated in the two transect valley profiles, AA' and BB' (Fig. 6). The aggradation/incision depths are ~ 60, ~ 260, ~ 60 and ~ 50 m for stages S1, S2, S3 and S4 respectively (Fig. 6).

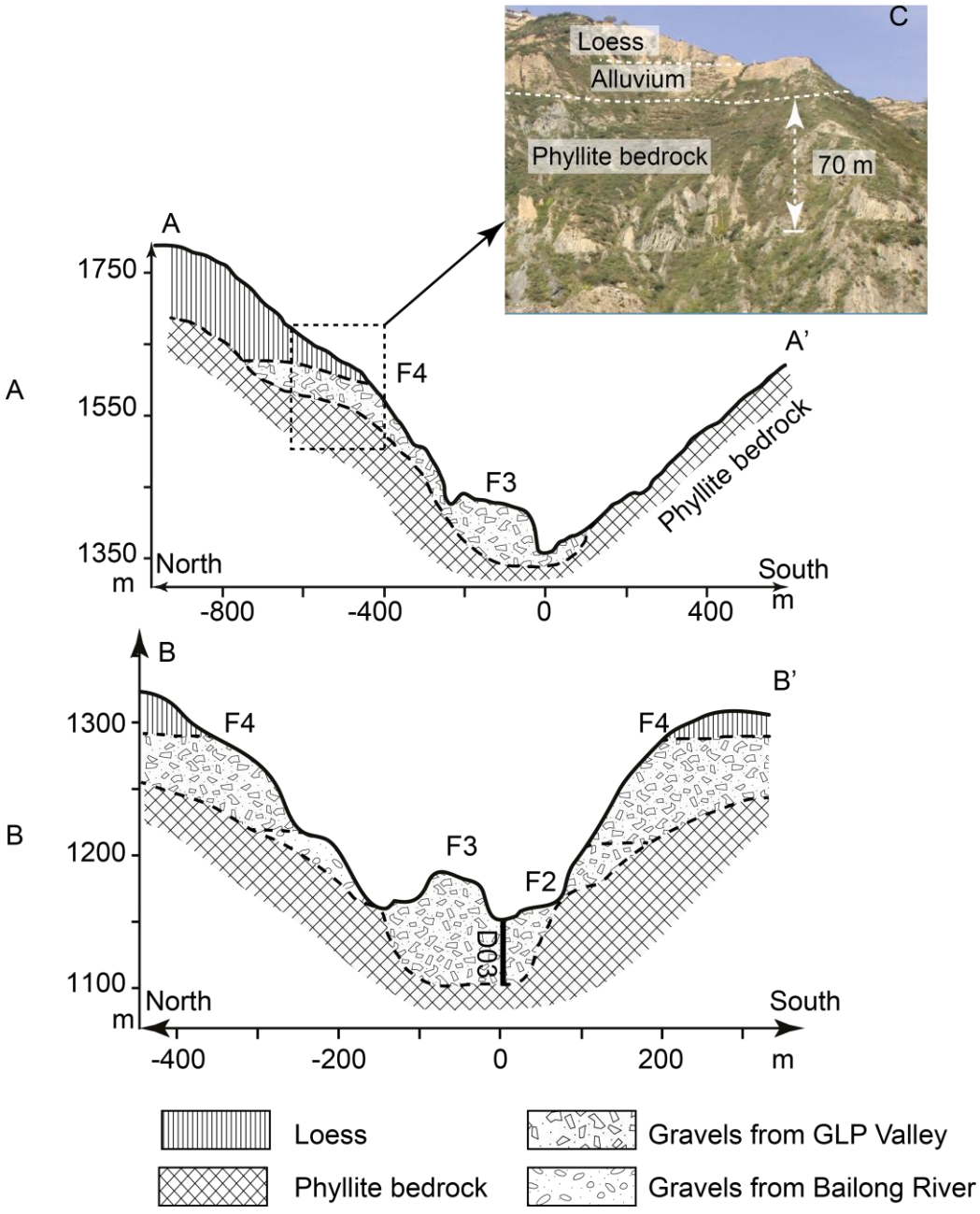

201

202 Fig. 6. Two cross-valley transects showing the spatial relationship between

203 different alluvial fan terrace levels. The location of the two profiles are shown in

204 Fig. 3.

3. Methods

3.1. Sampling and distribution of OSL samples

OSL dating is a chronometric technique that is commonly used to determine the time elapsed since a sedimentary quartz grain was last exposed to sunlight (Wintle, 2008). Because this exposure usually occurs while the grain is being transported prior to deposition at the sample site, OSL ages are usually interpreted as depositional ages. Because debris flows/debris-charged floods are energetic processes, usually leading to rapid deposition of coarse gravelly sediments, fine materials (<2 mm in diameter) are either difficult to sample from poorly sorted gravelly sediments or provide poorly bleached OSL signals. Therefore, we used the silt materials that were deposited by less-energetic processes for OSL dating. These materials include the alluvial silt intercalated between gravelly sediments, the paleosols capping the F2 and F3 alluvial fans/terraces, and the aeolian loess capping the F4 alluvial fans/terraces. These samples represent secondary low-energy fluvial/aeolian deposition during the intervals between debris flows/floods, and the ages of these samples were used to confine the periods during which alluvial fan/terrace aggradation occurred. In the field, samples were collected by hammering steel tubes (4 cm in diameter, and 25 cm in length) into vertical exposures. The two ends of the tubes were immediately sealed using foil, several layers of opaque plastic bags, and tape. Samples from the boreholes were collected by hammering a thin steel tube into

the muddy layers. These samples were subsequently sealed using the same method as described above. The locations of sample sites are displayed in Fig. 3, and the detailed distribution of OSL samples is displayed in Fig. 7. Four samples were taken from the F2 terraces, 12 from the F3 terraces, five from the F4 terraces and three from the boreholes.

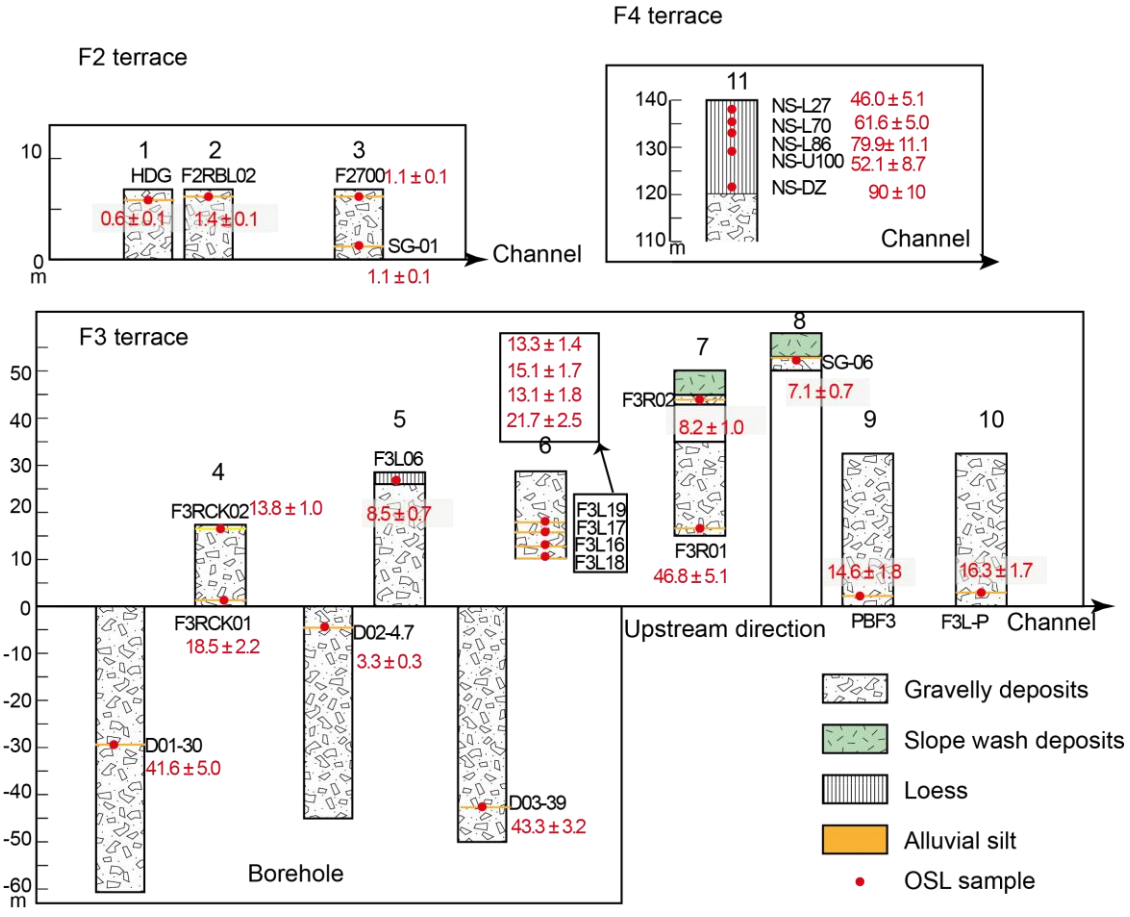

Fig. 7. Location of the OSL samples within each terrace profile or borehole. The vertical axis represents the elevation relative to the present channel. Upstream profiles are located on the right side of the figure, while downstream profiles are on the left. The numbers above each profile represent the locations of the profiles as shown in Fig. 3. The measured OSL ages are shown with red

numbers (ka).

3.2. Sample preparation and measurement

In the laboratory, the sunlight-exposed outer layers of sediments were removed and preserved for measurements of dose rate and water content. The unexposed portion was prepared for equivalent dose (D_e) determination. These unexposed samples were sequentially treated with HCl and H_2O_2 to remove carbonate and organic matter respectively. Using Stokes settling, the 4–11 μm fraction was obtained and subsequently treated with H_2SiF_6 to remove feldspars. The fine-grained (4–11 μm) quartz grains were mounted on aluminum discs for OSL measurement.

Equivalent doses (D_e) were measured using the Single Aliquot Regenerative dose (SAR) procedure (SM Table S1) of Murray and Wintle (2000). All measurements were performed using a Risø TL-DA-20 TL/OSL luminescence reader (Bøtter-Jensen et al., 2003). The reader utilizes a $^{90}Sr/^{90}Y$ beta source, calibrated by the method of Armitage and Bailey (2005), to perform laboratory irradiations. Optical stimulation was achieved using an array of light emitting diodes (LEDs) illuminating the sample at either 870 nm (infrared LEDs) or 470 nm (blue LEDs). Both stimulation sources were routinely operated at 90% current, giving measured power densities of 62.5 (480 nm) and 185.4 (870 nm)

mW/cm^2. The OSL signal was measured using an Electron Tubes Ltd 9235QA photomultiplier tube with 7.5 mm of Hoya U-340 filter. The OSL signal was integrated from the first 0.48 s with the averaged photon counts from the last 4 s subtracted as a background. All growth curves were fitted using a saturating exponential plus linear function because the loess samples capping the F4 alluvial fan provide large luminescence signals, which would lead to saturation if only using saturating exponential function (SM, Fig. S5). The Central Age model (Galbraith and Roberts, 2012) was used to produce sample D_e values. Twelve to 24 aliquots were measured for each sample. A 160 °C, 10 s preheat 1 (the preheat prior to measurement of the natural or regenerated luminescence signal) paired with a 160 °C cut-heat (the preheat prior to measurement of the test dose luminescence signal) was selected for equivalent dose measurement sequences on the basis of dose recovery tests (SM, Fig. S6).

The environmental dose rates were determined using a thick source alpha counter (TSAC) (i.e., Daybreak Model 583 Intelligent Alpha Counter), and a Risø GM-25-5A low-level beta GM multicounter system ("GM beta-counter"). For each sample, the ^{238}U and ^{232}Th concentrations were measured by the TSAC. The beta dose rates of these two radionuclides were calculated using the conversion factors of Adamiec and Aitken (1998). The beta dose rate of ^{40}K was obtained by subtracting from the total beta dose rate (obtained by the GM beta-counter)

278 the proportions of ^{238}U and ^{232}Th. The ^{40}K concentration was subsequently
279 obtained using the conversion factors of Adamiec and Aitken (1998). Finally, the
280 alpha, beta and gamma dose rates were calculated using the radionuclide
281 concentrations obtained above. Dry dose rates were corrected for alpha
282 efficiency (Rees-Jones, 1995) and alpha and beta attenuation (Mejdahl, 1979;
283 Bell, 1980). For samples collected above the present-day water table (which
284 yielded water contents of 5–6%), the water content was taken as 10 ± 5%, which
285 is approximately half of the saturated water content (~20%). This value was used
286 because terrace sediments tend to experience occasional saturation conditions
287 prior to terrace abandonment, with dewatering occurring after terrace
288 abandonment. For samples beneath the present-day water table, it is expected
289 that the sample has been in the saturated condition for most of the burial period,
290 therefore, the saturated water content was used. The cosmic dose rate was
291 obtained following Prescott and Hutton (1994). Dose rates, equivalent doses and
292 OSL ages, are presented in Table 1.

Table 1. OSL dating results. W is water content. σ is the over-dispersion value, and n is the number of accepted aliquots. For most samples in dry conditions upon sampling, the water content is taken as 10 ± 5% which is roughly a half of the saturated water content. For samples which are in wet conditions, their saturated water contents were measured in laboratory.

Sample	Origin	Radionuclide concentrations			Sample	W	Cosmic	Dose rate	Equivalent	(n)	σ	Age
		K (%)	U (ppm)	Th (ppm)	(m)	(%)	(Gy/ka)	(Gy/ka)	(Gy/ka)		(%)	(ka)
D01-30	Alluvial	1.64 ± 0.36	3.94 ± 0.34	4.03 ± 1.2	30 ± 0.2	20.2 ± 2	0.02 ± 0.00	2.90 ± 0.31	120.7 ± 6.3	23	25	41.6 ± 5.0
D02-4.7	Alluvial	2.08 ± 0.42	3.47 ± 0.45	9.31 ± 1.59	4.7 ± 0.2	20.3 ± 2	0.14 ± 0.01	3.68 ± 0.36	12.2 ± 0.4	10	9.4	3.3 ± 0.3
D03-39	Alluvial	1.72 ± 0.17	3.05 ± 0.31	9.89 ± 0.99	39 ± 0.2	22.4 ± 2	0.02 ± 0.00	3.13 ± 0.22	135.6 ± 2.6	21	8.1	43.3 ± 3.2
F2700	Paleosol	1.86 ± 0.41	3.81 ± 0.44	6.62 ± 1.52	0.5 ± 0.2	10 ± 5	0.22 ± 0.01	3.79 ± 0.39	4.1 ± 0.1	22	12	1.1 ± 0.1
SG-01	Alluvial	1.86 ± 0.41	3.81 ± 0.44	6.62 ± 1.52	5.0 ± 0.2	10 ± 5	0.12 ± 0.01	3.26 ± 0.19	2.7 ± 0.2	15	24	0.8 ± 0.1
F2RBL02	Alluvial	2.22 ± 0.45	3.19 ± 0.54	11.67 ± 1.86	1.0 ± 0.2	10 ± 5	0.2 ± 0.01	4.37 ± 0.43	6.1 ± 0.1	23	4.4	1.4 ± 0.1
HDG	Alluvial	2.37 ± 0.45	3.27 ± 0.51	10.3 ± 1.79	0.5 ± 0.2	10 ± 5	0.21 ± 0.01	4.42 ± 0.43	2.8 ± 0.1	18	7.5	0.6 ± 0.1
F3RCK01	Paleosol	1.66 ± 0.17	2.3 ± 0.23	10.84 ± 1.08	1.0 ± 0.2	10 ± 5	0.2 ± 0.01	3.49 ± 0.24	48.0 ± 0.8	20	6.8	13.8 ± 1.0
F3RCK02	Alluvial	1.39 ± 0.3	2.59 ± 0.33	7.51 ± 1.16	17.0 ± 0.2	10 ± 5	0.04 ± 0.00	2.86 ± 0.3	53 ± 2.9	18	23	18.5 ± 2.2
F3L06	Paleosol	1.74 ± 0.23	2.1 ± 0.33	9.78 ± 1.45	0.5 ± 0.2	10 ± 5	0.22 ± 0.01	3.41 ± 0.27	29.0 ± 0.4	18	4.9	8.5 ± 0.7
F3L16	Alluvial	1.52 ± 0.37	5.31 ± 0.51	5.63 ± 1.78	15.0 ± 0.2	10 ± 5	0.04 ± 0.00	3.71 ± 0.42	48.7 ± 3.8	20	35	13.1 ± 1.8
F3L17	Alluvial	1.68 ± 0.36	4.3 ± 0.4	5.64 ± 1.39	14.0 ± 0.2	10 ± 5	0.05 ± 0.00	3.53 ± 0.37	53.3 ± 1.5	21	12	15.1 ± 1.7
F3L18	Alluvial	1.18 ± 0.31	3.61 ± 0.37	6.31 ± 1.32	16.0 ± 0.2	10 ± 5	0.04 ± 0.00	2.9 ± 0.32	62.9 ± 1	23	6.4	21.7 ± 2.5
F3L19	Alluvial	1.76 ± 0.36	2.97 ± 0.44	10.4 ± 1.52	13.0 ± 0.2	10 ± 5	0.05 ± 0.00	3.61 ± 0.36	47.9 ± 1.4	24	13	13.3 ± 1.4
F3R01	Alluvial	1.92 ± 0.41	4.53 ± 0.45	5.45 ± 1.57	8.0 ± 0.2	10 ± 5	0.09 ± 0.00	3.85 ± 0.41	180.3 ± 2.1	24	1.8	46.8 ± 5.1
F3R02	Alluvial	0.76 ± 0.29	4.43 ± 0.48	6.14 ± 1.63	5.0 ± 0.2	10 ± 5	0.12 ± 0.01	2.85 ± 0.35	23.4 ± 0.2	24	2.3	8.2 ± 1.0
PB-F3L	Alluvial	1.93 ± 0.42	4.31 ± 0.54	9.73 ± 1.89	10.0 ± 0.2	22.4 ± 2.2	0.07 ± 0.00	3.7 ± 0.38	60.2 ± 0.5	23	0.8	16.3 ± 1.7
F3L-P	Alluvial	1.46 ± 0.37	3.73 ± 0.47	9.66 ± 1.65	8.0 ± 0.2	10 ± 5	0.09 ± 0.00	3.55 ± 0.38	51.9 ± 2.8	11	16	14.6 ± 1.8
SG-06	Alluvial	2.87 ± 0.52	3.54 ± 0.5	11.7 ± 1.76	2.0 ± 0.2	10 ± 5	0.18 ± 0.01	5.06 ± 0.49	36.1 ± 0.5	10	1.3	7.1 ± 0.7
NS-L27	Loess	1.62 ± 0.4	4.6 ± 0.48	5.52 ± 1.65	2.7 ± 0.2	5 ± 2	0.17 ± 0.01	3.86 ± 0.42	177.6 ± 2.8	24	5.6	46.0 ± 5.1
NS-L70	Loess	1.93 ± 0.26	3.04 ± 0.41	10.27 ± 1.45	7.0 ± 0.2	5 ± 2	0.1 ± 0.00	4.02 ± 0.32	247.3 ± 3.2	26	3.4	61.6 ± 5.0
NS-86	Loess	1.71 ± 0.58	3.17 ± 0.39	9.31 ± 1.37	8.6 ± 0.2	5 ± 2	0.08 ± 0.00	3.74 ± 0.51	299 ± 8.5	12	8.8	79.9 ± 11.1
NS-U100	Paleosol	1.75 ± 0.61	3.60 ± 0.49	8.36 ± 1.73	10.0 ± 0.2	5 ± 2	0.08 ± 0.00	3.84 ± 0.54	200 ± 18	8	25	52.1 ± 8.7
NS-DZ	Loess	1.42 ± 0.35	3.3 ± 0.41	8.26 ± 1.41	2.0 ± 0.2	5 ± 2	0.18 ± 0.01	3.50 ± 0.36	315 ± 13	14	14	90 ± 10

4. Results

A total of 24 samples were dated. For the F4 alluvial fans/terraces, five loess samples (NS-L27, NS-L70, NS-86, NS-U100 and NS-DZ) were taken and dated from one loess profile overlying the F4 alluvial fan at the downstream end of the GLP River (Fig. 7). The ages for samples NS-L27, NS-L70 and NS-L86 are in stratigraphic order, and the D_e values are characterized by low over-dispersion values (Table 1, 3.4–8.8%) consistent with aeolian deposition (Lai, 2006; Lai et al., 2007; Stevens et al., 2008). Conversely, the over-dispersion value for sample NS-U100 is relatively high for aeolian material (25%), and its OSL age does not fit in the stratigraphic order (Fig. 7). The cause of this discrepancy is unclear from these results alone, but it is possibly caused by post-depositional mixing. Sample NS-U100 was taken from a layer interpreted as a paleosol owing to its color and structure (dark reddish brown (5YR 3/3) silty clay with blocky structure), which in other luminescence studies of loess paleosols has resulted in inaccurate ages in some soil units (Stevens et al., 2008). Consequently, the age for sample NS-U100 is regarded as likely unreliable. Sample NS-DZ was taken from the base of the loess profile (Fig. 7). It yields an OSL age, 90 ±10 ka, which fits in the stratigraphic order. Because the D_e value is so high (315 Gy), and we know that quartz OSL ages from loess tends to yield age underestimates at such high doses (Buylaert et al., 2007; Lai, 2010; Chapot et al., 2012), the OSL age of 90.0±10.0 ka is regarded as a minimum estimate of its true burial age.

For the F3 terraces/fans, a total of 12 samples were dated. Sample F3L16, F3L17, F3L18 and F3L19 were taken from a single F3 terrace profile, and they produce stratigraphically consistent OSL ages between 21.7 ± 2.5 and 13.3 ± 1.4 ka (Fig. 7 and Table 1). Samples F3RCK01 and F3RCK02 were taken from a same F3 terrace at the mouth of the GLP valley (Fig. 7). Sample F3RCK02 produces an OSL age of 13.8 ± 1.0 ka with an over-dispersion value of 6.8%. Sample F3RCK01 produces an OSL age of 18.5 ± 2.2 ka with an over-dispersion value of 23%. The OSL ages for these two samples are in stratigraphic order. Samples F3R01 and F3R02 were taken from a single F3 terrace. The ages of F3R01 and F3R02 are 46.8 ± 5.1 ka and 8.2 ± 1 ka respectively, and they both have low over-dispersion values of about 2% (Table 1). Noticeably, the age of F3R01 (46.8 ± 5.1 ka) is much higher than the ages of samples taken from the other F3 terraces. The gravels overlying sample F3R01 are generally coated by a layer of dark varnish (Fig. 8), while the gravels at other F3 alluvial terraces do not have varnish. We interpret this dark varnish layer as indicating a relatively old F3 terrace that has been mostly eroded, leaving relics at this location. In addition, the age of F3R01 is close to that of sample D03-39, which was taken from 39 m beneath the present channel close to the bedrock valley floor (Fig. 7). Interestingly, the phyllite bedrock is exposed in the opposite side of the valley at the F3R01 location (Fig. 8). It is likely, therefore, that the position of F3R01 is also close to the phyllite bedrock. Overall, we consider the age of F3R01 as accurate. The remaining samples (i.e., SG-06, PB-F3L01, F3L-P and F3L06)

were each taken from separate F3 terraces (Fig. 7). These four samples provide OSL ages that are within the age ranges provided by the F3 terrace samples previously described, and are, therefore, accepted as broadly accurate.

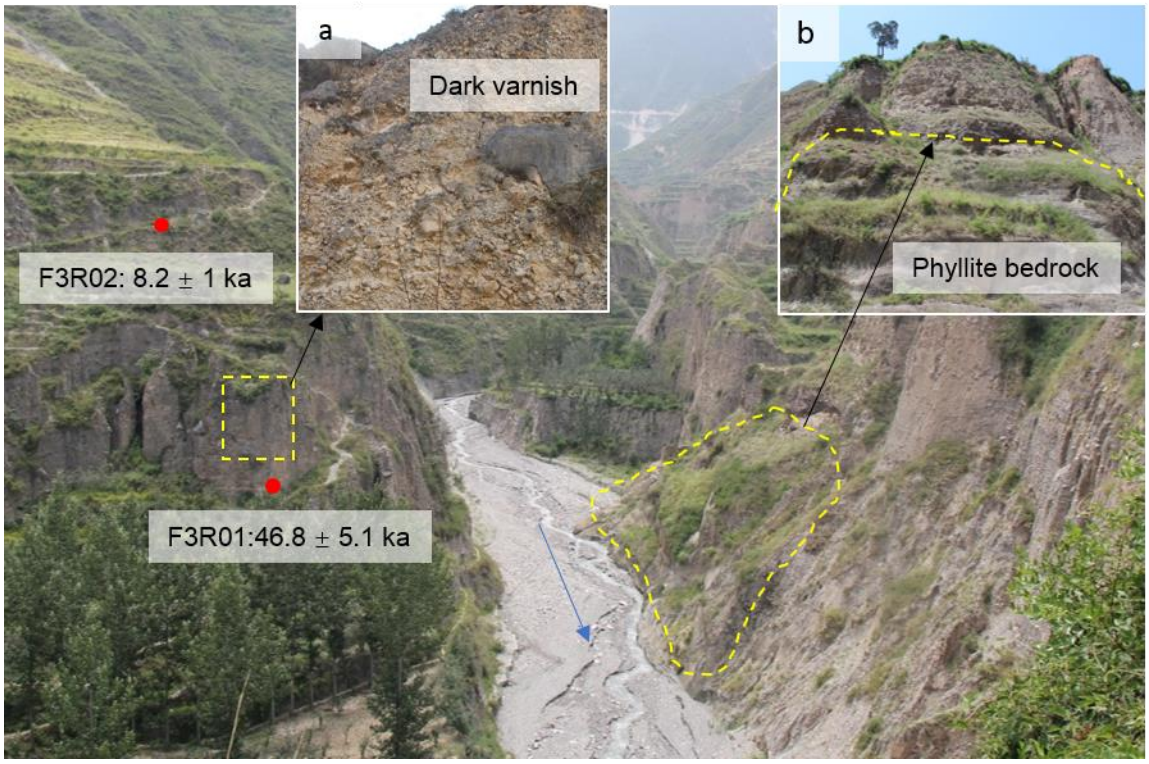

Fig. 8. Geological context of samples F3R01 and F3R02. The boulder and the surrounding gravels are coated with a dark varnish layer (inset photograph a). On the opposite side of the valley at the F3R01 location, the phyllite bedrock is present above the modern channel floor (inset photograph b).

Four samples were taken from the F2 terraces for OSL dating. Samples F2RBL02 and HDG were taken from separate F2 terraces (Fig. 7) and provide D_e values of 6.05 Gy and 2.79 Gy, respectively, with low over-dispersion values

(Table 1). These D_e values likely indicate satisfactory OSL signal resetting upon deposition. Samples F2700 and SG-01 were taken from the same F2 terrace location (Fig. 7). They both produce low D_e values of 4.05 Gy for F2700 and 2.66 Gy for SG-01 (Table 1). The OSL ages for F2700 and SG-01 are 1.07 ± 0.11 ka and 0.77 ± 0.07 ka, respectively (Fig. 7), which are identical within two sigma errors. Similarly, these two ages indicate that no significant residual OSL signals remained at deposition. Overall, the D_e and OSL ages for the sediments of the F2 terraces indicate that they were well-bleached prior to deposition and are suitable for OSL dating.

Three samples were taken from the boreholes (Fig. 7). Sample D01-30 was taken from 30 m beneath the present channel at borehole D01, sample D02-4.7 from 4.7 m at D02, and sample D03-39 from 39 m at D03. The OSL age for D01-30 is 41.6 ± 5.0 ka with a relatively high over-dispersion value of 25%. Sample D03-39 yields an OSL age of 43.3 ± 5.0 ka with an over-dispersion value of 8.1%. These two samples (i.e., D01-30 and D03-39) are located at similar depths beneath the present channel, and they both produce similar ages. Therefore, these ages are accepted as broadly accurate. Sample D02-4.7 produces an OSL age of 3.3 ± 0.3 ka with an over-dispersion value of 9.4%. This OSL age is also in stratigraphic order with those of the two other borehole samples and is also considered a broadly accurate estimate of the burial ages.

373 Above all, consideration of the sample stratigraphy indicates that alluvial silt
374 deposited by slow overbank flows, paleosols, and loess provide accurate
375 estimates of the sample burial ages and are, therefore, satisfactory materials for
376 OSL dating.

377 **5. Discussion**

378 *5.1. Timing of aggradation and incision phases*

379 The timing of phases of aggradation and incision is critical to understanding the
380 causes of sedimentation and erosion in GLP, which is hypothesized to be
381 representative of much of the middle portion of the Bailong Valley. Here, the time
382 of the beginning and end of each identified aggradation/incision period is
383 confined using the OSL ages described above.

384

385 The F4 alluvial fans/terraces were deposited during the earliest aggradational
386 phase identified in GLP, termed the S1 aggradational phase. The end of the S1
387 phase is defined by the OSL age for sample NS-DZ, which was taken from the
388 top of the F4 terrace and yields an OSL age of 90.0 ± 10.0 ka (Fig. 7). This
389 represents a maximum age for the termination of the S1 aggradation phase.
390 However, the start of the S1 aggradation period has yet to be determined
391 because it was not possible to obtain OSL samples from the base of the F4
392 terraces.

Sediments from both the base and top of the F3 terraces have been dated, which allows an estimate of the duration of the S3 aggradation period. The samples from the top of the F3 terraces include F3L06, F3R02 and SG-06 (Fig. 7). These samples provide OSL ages between 8.5 ± 0.7 ka and 7.1 ± 0.7 ka (Table 1), which are essentially indistinguishable, indicating a consistent date for the cessation of aggradation. However, sample F3RCK02, which was taken from the top of the F3 alluvial fan at the valley mouth (Fig. 7), provides an OSL age of 13.8 ± 1.0 ka, older than the three samples located on the top of the F3 terraces. This age is similar to those of samples F3L16, F3L17 and F3L19 (Fig. 7), which were taken from the middle portion of the F3 terrace profile. Obviously, when the F3 terraces in the upstream portion of the valley continued experiencing aggradation after 13.8 ± 1.0 ka, the F3 alluvial fan at the valley mouth was abandoned. It is likely that the abandonment of the F3 alluvial fan was caused by channel avulsion. Therefore, the age of sample F3RCK02 does not represent the end of the S3 phase aggradation. The youngest age, 7.1 ± 0.7 ka, is taken to define the latest end of S3 phase aggradation. The timing of the beginning of aggradation is estimated from the age of sample F3R01 (46.8 ± 5.1 ka). This age is indistinguishable from that of sample D03-39 m (43.3 ± 3.2 ka), which is 39 m beneath the current downstream GLP alluvial channel floor from core D03 (Fig. 7). The ages of these two samples indicate that the GLP bedrock

414 channel beneath the current alluvial channel formed at least before 46.8 ± 5.1
415 ka, and that the valley has experienced long-term aggradation since then
416 forming the widespread F3 terraces. It is deduced that this aggradation had been
417 interrupted by some short-term incision events leaving terrace relics older than
418 the exposed F3 terraces, as is indicated from the OSL age of sample F3R01.

419

420 Overall, the S3 aggradational phase appears to occur between 46.8 ± 5.1 ka
421 and 7.1 ± 0.7 ka and is responsible for the formation of the exposed F3 alluvial
422 fans/terraces and the alluvium underlying the current channel floor. The lower
423 age (46.8 ka ± 5.1 ka) is a minimum estimate of the onset of aggradation
424 because the sample (F3R01) was taken at an unknown distance above the
425 phyllite bedrock, and the start of aggradation must predate this OSL age. As
426 noted above, the upper age (7.1 ± 5.1 ka) is a maximum age estimate for the
427 termination of aggradation.

428

429 Periods of incision, termed S2 and S4, occurred between the S1 and S3 periods
430 of aggradation, and after S3. Therefore, the S2 period must have occurred
431 between 90.0 ± 10.0 ka and 46.8 ± 5.1 ka, and the S4 period between 7.1 ± 0.7
432 ka and the present. Both time ranges represent the maximum duration of incision.
433 During the S4 incision period, telescopic alluvial fans (F1 and F2) formed in the
434 distal ends of the F3 alluvial fans. These alluvial fans/terraces likely represent

periods of partial-buffering when sediments sourced from the limestone headwaters were transported through the incised F3 alluvial fans/terraces and deposited when coming out of the F3 alluvial fans. The ages of the four samples from the F2 terraces (i.e., HDG, F2RBL02, F2700 and SG-01) confine the aggradation time for F2 alluvial fan in a range of 1.4 ± 0.1 to 0.6 ± 0.1 ka (Fig. 7). As these samples were taken from sediments close to the surface of the F2 terraces (Fig. 7), we argue that the OSL ages represent the termination of F2 fan formation, though again it is possible that erosion of surficial material may have truncated the record of sediment deposition. The base of the F2 terraces is not determined because no clear stratigraphic boundary is found in the exposed F2 terraces. Nevertheless, sample D02-4.7, which was taken at a depth of 4.7 m in core D02 beneath the current GLP channel (Fig. 7), produces an OSL age of 3.3 ± 0.3 ka. This age suggests that debris flow/debris-charged deposition have occurred after this time. Therefore, the deposition of the F2 alluvial fan is confined between 3.3 ± 0.3 ka and 0.6 ± 0.1 ka. The time of the F1 alluvial fan formation is not confined because no fine silt was sampled from these F1 alluvial fans.

5.2. Relationships between climate and alluvial fan/terrace aggradation/incision phases

We used a composite speleothem record from Hulu Cave (Wang et al., 2001) and Sanbao Cave (Wang et al., 2008) to represent the climate during the

timeframe represented by sediments in GLP. The speleothem $\delta^{18}O$ record is regarded as recording the strength of the East Asian Summer Monsoon (EASM) on orbital timescales (Wang et al., 2008; Wang et al., 2017). The general climatic conditions since the last interglacial period were summarized on the basis of pollen records (Li et al., 1988) into three characteristic phases of monsoon operation: the warm wet interglacial and Holocene pattern (MIS 5 and 1), the cold wet transitional interstadial pattern (MIS 3) and the cold dry full glacial pattern (MIS 2 and 4).

The climatic records are compared with the aggradation and incision stages observed in the GLP valley in Fig. 9. Because the ages for the S1 and S2 periods are not tightly constrained, the relationship between phases S1 and S2 and the climatic condition is not discussed here. The S3 aggradation phase falls in two different climate periods (i.e., MIS 3 and MIS 2), possibly indicating a weak correlation between climate and alluvial fan aggradation. These two climatic periods both represent a cold condition as is suggested from the pollen records from nearby area (Li et al., 1988). It is likely that cold conditions were responsible for the aggradation in these periods. Cold conditions, together with the well-developed inter-crossing joints in the limestone bedrock, might enhance frost shattering (Walder and Hallet, 1985; Anderson, 1998; Hales and Roering, 2007; Herman and Champagnac, 2016) in the high-elevation limestone areas (Fig. 3a),

leading to increased rockfall activity and abundant supply of angular clasts. These angular clasts may be transported from the limestone hillslopes to the relatively low-elevation phyllite area during infrequent rainfall storms, resulting in deposition of alluvial terraces/fans. The Bailong River region is characterized by intense rainfall events during summer seasons at present, and a total of 107 rainstorm events (daily precipitation>50 mm) have been recorded between 1961 and 2000 (Fan, 2006). It is expected that the frequency of the rainstorm events during weak EASM periods is lower than that of the present strong EASM period (Liang et al., 2010). Each individual rainstorm event may contribute to the depletion of sediments in the form of debris flows or debris-charged floods.

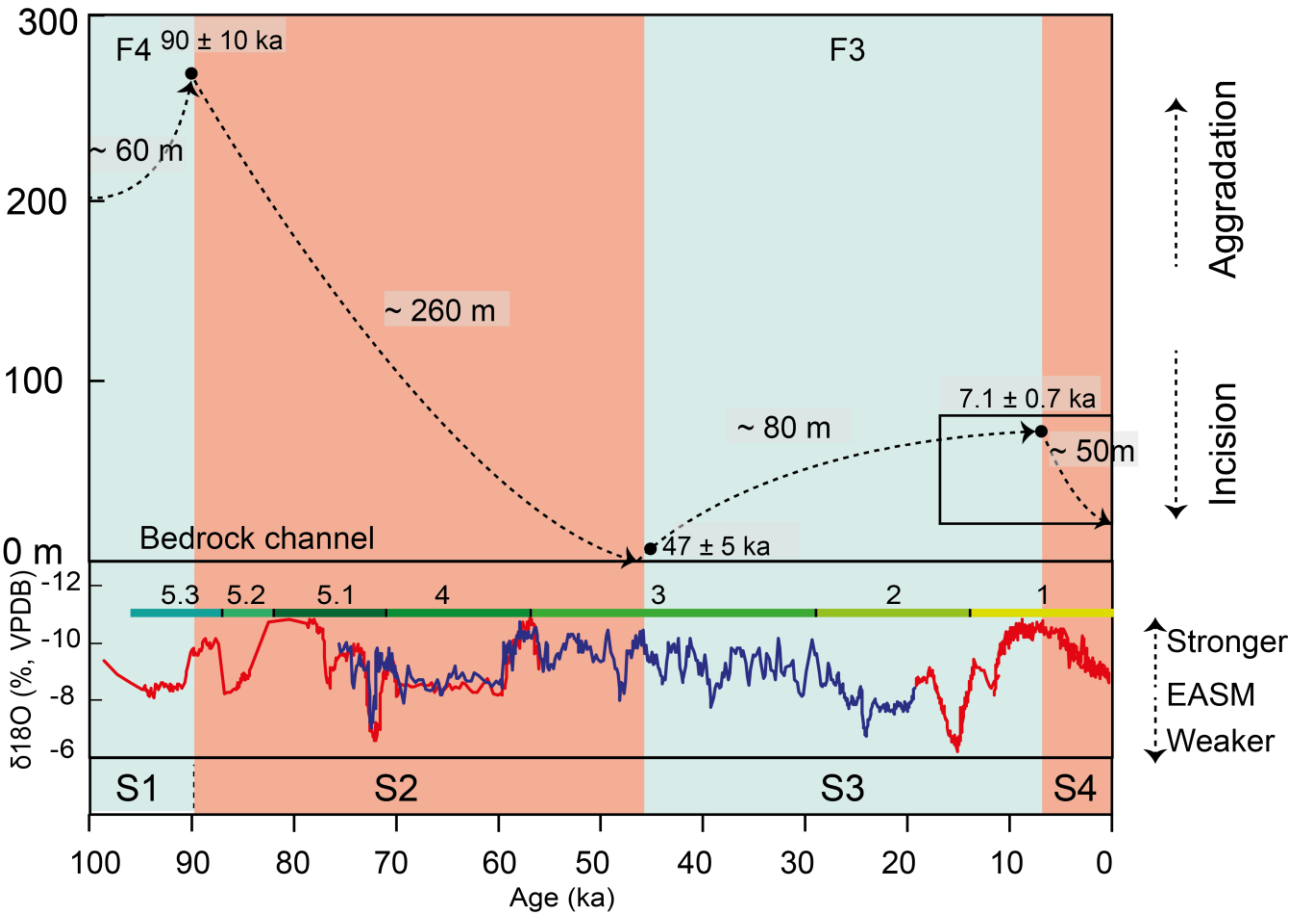

Fig. 9. GLP aggradation/incision stages and speleothem $\delta^{18}O$ records. Filled dots represent OSL ages that define the corresponding aggradation or incision period. Red curves are the Sanbao Cave $\delta^{18}O$ speleothem records (Wang et al., 2008), and blue curves are the Hulu Cave records (Wang et al., 2001). The numbers and colored bars above the speleothem curves are Marine Oxygen Isotopic Stages (Lisiecki and Raymo, 2005). Black dashed lines define the evolution stages in profile A-A'. Black dashed lines with an upward pointing arrow represent the aggradation of the corresponding alluvial fans, and black dashed lines with a downward pointing arrow represent the incision of the previous alluvial fans. The blue shading represents aggradation periods, and the pink

499 shading represents incision periods. The box on the right of the figure is enlarged
500 in Fig. 10.

501

502 The S4 incision occurred in the mid-Holocene period, during which the
503 speleothem record shows a slight weakening of the EASM strength (Fig. 9).
504 However, a number of studies (An et al., 2003; Lu et al., 2013; Wang et al., 2014;
505 Chen et al., 2015) have shown that the mid-Holocene may have been
506 characterized by warm and wet conditions, contrasting with the cave records. It
507 is likely that the general pattern of glacial and interglacial change may be broadly
508 reflected in Chinese $\delta^{18}O$ speleothem records (Wang et al., 2017), while the
509 speleothem records do not represent the true variation of the EASM at millennial
510 scales, especially since Last Deglaciation (Maher and Thompson, 2012; Tan,
511 2014; Liu et al., 2015; Yang et al., 2016) . Here, we used a pollen record covering
512 the past 14 ka from Gonghai Lake (Chen et al., 2015) to represent the variation
513 of EASM strength since Last Deglaciation in northern China (Fig. 10). According
514 to this figure, the S4 incision corresponds to a mid-Holocene warm and wet
515 climate. Pollen records from the nearby southwest Loess Plateau revealed that
516 a desert-steppe during the period between 11,190 and 8850 yr BP was
517 succeeded by a forest-steppe from 8850 to 7540 yr BP, a Pinus-dominated forest
518 from 7540 to 6560 yr BP, and a deciduous forest from 6560 to 5790 yr BP (Feng
519 et al., 2006). This transition of vegetation indicates that the climate changed to

warmer and wetter conditions in the mid-Holocene. It is likely that the limestone hillslopes in GLP were covered by a forest vegetation similar to the present during the mid-Holocene. This vegetation cover may stabilize the sediments on the hillslopes and reduce bedrock weathering rates, leading to decreased supply of sediment. Meanwhile, annual water discharges and the frequency of flood discharges may increase during the warm and wet period (Knox, 1993; Fowler and Hennessy, 1995), leading to flows that exceed the critical stream power (Bull, 1991) and produce incision.

According to this record, it is also clear that since 3.3 ka, the climate has started to become drier (Fig. 10). The vegetation in the nearby southwest Loess Plateau changed to a steppe from 4000 to 3120 yr BP and then to a desert-steppe from 3120 to 2900 yr BP (Feng et al., 2006). It is likely that the F2 aggradation was caused by increased sediment availability due to reduced vegetation cover resulting from the aridity. The formation of the F2 terraces/fans likely continued until the climate became wet again as is reflected from the sharp increase in the reconstructed precipitation in around 1 ka (Fig. 10). Likewise, the F1 alluvial fan formed in a second dry period, though here we did not obtain OSL ages for the F1 terraces.

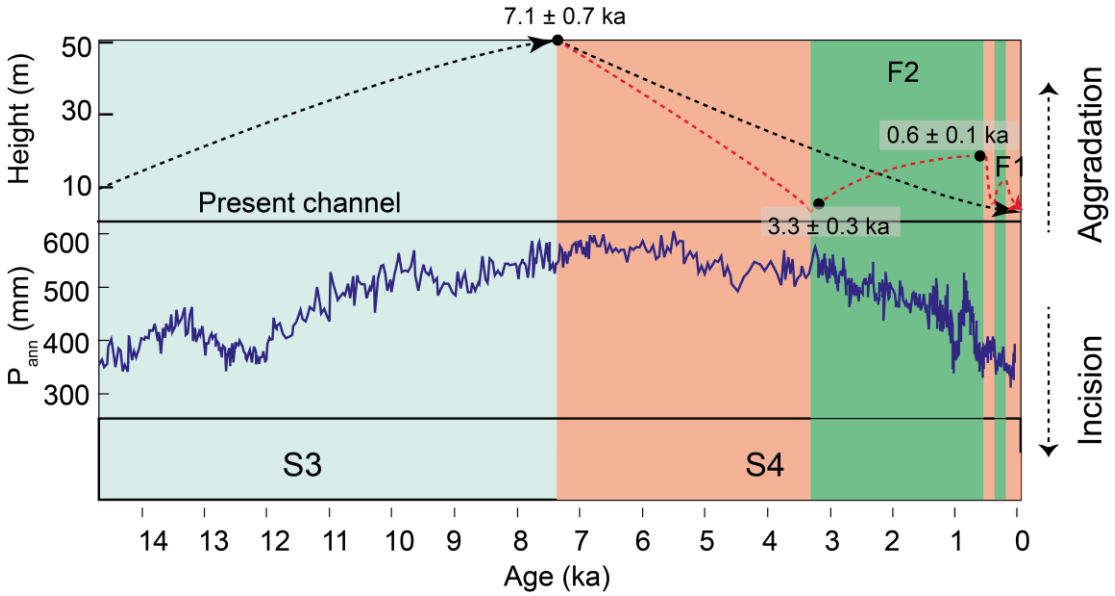

Fig. 10. GLP aggradation/incision stages and pollen records. Filled dots are OSL ages that define the corresponding aggradation or incision period. The blue curves are pollen-based precipitation records from Gonghai Lake (Chen et al., 2015). Black dashed lines define the evolution stages in the proximal area of alluvial fans. Black dashed lines with an upward pointing arrow represent the aggradation of the corresponding alluvial fans. Black dashed lines with a downward pointing arrow represent the incision of the previous alluvial fans. Dashed red lines define the evolution stages in the distal fan area, representing two small aggradation periods forming the F2 and F1 alluvial fans. The blue shading represents aggradation periods, the pink shading represents incision periods, and the green shading represents the small aggradation period.

From the discussion above, it is concluded that cold environments tend to

553 enhance frost shattering, while dry environments generally cause reduced
554 vegetation cover. Both effects contribute to a high sediment supply rate, leading
555 to alluvial fan aggradation during infrequent flood discharge events. Conversely,
556 a warm and wet climate causes a reduction in sediment supply due to recovered
557 vegetation and an increase of the frequency of flood discharges, leading to
558 alluvial fan/terrace incision. Similar relationships between climate and
559 aggradation/incision patterns have been found in fluvial terraces in the marginal
560 area of the Tibetan Plateau (Wang et al., 2009; Lu et al., 2010; Huang et al.,
561 2014; He et al., 2015). This similarity suggests that the GLP valley might respond
562 to the climate in a similar manner to the primary rivers in the study area. Many
563 studies have argued that alluvial fan deposition occurred during periods of
564 climatic transitions because great changes in flood magnitude/frequency and
565 vegetation may occur during these periods (Bull, 1991; MacDonald et al., 2003).
566 In this study, samples of glacial ages (21-16 ka) and glacial-interglacial transition
567 ages (13-7 ka) were obtained, indicating aggradation in both glacial and glacial-
568 interglacial transition periods. This situation is consistent with the traditional
569 expectations for fan aggradation during climatic transition periods. In addition,
570 as the GLP valley is among the typical valleys in the middle section of the Bailong
571 River, representing intermediate-sized tributary valleys (10 – 100 km^2) with
572 relatively large alluvial fan areas and limestone drainage headwaters, the
573 relationships between fan evolution and climate may apply to similar types of
574 valleys in the other sections of the Bailong River.

575 It is noteworthy that different relationships between fan evolution and climatic
576 conditions have been discovered in other parts of the eastern Tibetan Plateau.
577 For example, Chen et al. (2008) found alluvial fan formation during 10.6–5.4 ka,
578 corresponding to a transition towards a more warm and humid climate in the
579 southeast of the Tibetan Plateau. Actually, contrasting relationships between
580 climate and alluvial fan evolution are present in many areas across the globe
581 (Bull, 1991, 2000; Owen et al., 1997, 2014; Harvey et al., 1999; Kumar et al.,
582 2007; Spelz et al., 2008; Juyal et al., 2010; Kar et al., 2014). One explanation is
583 the variable geomorphic thresholds for different types of valleys (Schumm, 1979;
584 Blair and McPherson, 1994; Coulthard et al., 2005; Phillips, 2006). The
585 difference in geomorphic thresholds may lead to distinct responses to the same
586 climatic events (Wells and Harvey, 1987; Wilford et al., 2004; Jakob, 2005),
587 leading to distinct evolutionary stages of alluvial fans. Moreover, climate-
588 associated parameters (i.e. precipitation, temperature and vegetation) may be
589 different across the northern and southern parts of the eastern Tibetan Plateau.
590 For example, the southern part may receive more precipitation than the north
591 does (Liang et al., 2010). This difference may lead to distinct valley evolution
592 stages corresponding to glacial/interglacial periods. Similar conditions have
593 been reported in the America Southwest (e.g., Harvey et al., 1999; Miller et al.,
594 2010), where even though climate is generally characterized by cold-wet and
595 warm-dry conditions in glacial and interglacial periods, respectively, the northern
596 and southern part of the America Southwest experiences distinct vegetation

cover and annual precipitations, leading to different climate-alluvial fan dynamic models. In other cases, the propagation of the effect of base-level change, which may be caused by river capture or regional uplift, also leads to differential evolutionary stages of alluvial fans across a region. One example is the alluvial fans in the Tabernas Basin in southeastern Spain where an uplift-induced base-level fall leads to the propagation of incision from the lower part of the basin to the upper part (Mather et al., 2017). Perhaps more importantly, variations in bedrock structures that control sediment delivery may also lead to differences in fan evolution (Mather and Stokes, 2017). Having considered these factors (specifically the localized bedrock structures), it is possible that some variations of alluvial fan/terrace evolution among the intermediate-sized valleys may also occur. It is suggested that future research on the correlation of alluvial fans/terraces across different valleys in the middle section of the Bailong River is needed.

5.3 The effects of the Bailong River and human activity on fan/terrace evolution

Although this study focused on the impact of climate on alluvial fan evolution, some local factors, such as the Bailong River and human activities, may also influence fan evolution. The effects of these factors are discussed briefly here.

5.3.1. Effect of the Bailong River

As the alluvial fans in GLP are of a tributary-junction type that are subject to the

617 lateral erosion and/or vertical incision of the axial river (Mather et al., 2017), the
618 Bailong River is potentially a factor in affecting alluvial fan dynamics. According
619 to our observations in the valley, valley incision is mainly triggered by flooding
620 events, i.e., a proximal-induced coupling regime (Mather et al., 2017). It is
621 suggested that the distally-induced incision is a secondary factor causing fan
622 incision. Moreover, as is suggested before, the GLP valley responded to climatic
623 changes in a similar manner to the primary rivers in the eastern Tibetan Plateau.
624 It is likely that during satisfactory climatic conditions both the Bailong River and
625 the GLP valley experience incision, and hence both distally-induced and
626 proximally-induced coupling (Mather et al., 2017) may occur, leading to rapid
627 incision. In contrast, during periods when the Bailong River is not being incised,
628 lateral migration of the river channel may create or destroy the accommodation
629 space of alluvial fans, leading to fan progradation or fan cutting, respectively.
630 The formation of the F1 and F2 alluvial fans were likely formed when the Bailong
631 River moved away from the GLP valley, creating space for gravelly sediments to
632 be deposited, though the fan formation was associated with a drying trend of the
633 climate as is discussed earlier. Moreover, the distal ends of the F1 and F2 alluvial
634 fans display a linear shape (Fig. 3), indicating periods when the Bailong River
635 approached the GLP valley and caused lateral erosion of the GLP alluvial fans.

636 *5.3.2. Effect of human activities*

637 As residents have utilized these alluvial fans/terraces as agricultural and

638 residential lands, human activities may exert an impact on past fan evolution,
639 especially for the young F1 and F2 fans/terraces. Activities associated with
640 agriculture primarily include surface flattening and vegetation removal on alluvial
641 fans/terraces to make space for crops. These agricultural activities may lead to
642 unstable terrace surfaces, causing surface erosion. Other activities such as
643 forest harvest and rock mining in the limestone headwaters may form unstable
644 hillslope surfaces and increase sediment supply in the limestone headwaters.
645 These activities may contribute to alluvial fan/terrace formation. The F1 and F2
646 alluvial fans/terraces, which are estimated to have been formed since about 3
647 ka, may be influenced by these activities.

648 *5.4. Implications for debris flow/debris-charged flood hazard*

649 The GLP valley, as well as the wider Bailong River region, is affected by debris
650 flows and debris-charged floods at present. When gravelly sediments are
651 deposited on alluvial fan surfaces that support populations, significant hazards
652 can be produced. One example is the Zhouqu debris flow, which killed 1760
653 people (Tang et al., 2011). These devastating events are usually triggered by
654 heavy rainfalls during summer seasons between May and September. In
655 assessing the probability of hazards for a given alluvial fan, the trend of
656 aggradation and incision of the fan is crucial. Incision tends to deepen the
657 channel, leading to abandonment of alluvial fans and reducing the impact of
658 debris flows/debris-charged floods on local populations (living on alluvial fan

surfaces), while aggradation tends to elevate the channel floors and expose the population to the influence of debris flows/floods, hence increasing the hazard probability.

The evolutionary history of the GLP valley and its relationship to climate indicates that cold and/or dry environments tend to cause aggradation, while humid and warm environments tend to cause incision. Here, we attempt to apply this relationship to the prediction of future valley evolution with an aim of assessing debris flow/debris-charged flood hazards. To do this, we analyzed the trend of precipitation and temperature anomalies over the past 62 yr (1950-2012) from a nearby meteorological station (Fig. 11). During this period annual temperatures have experienced a measurable increase, particularly from c. 1980, while the annual precipitation is largely unchanged. The warming, which has occurred primarily in the winter for most of China (Hu et al., 2003), would tend to decrease frost shattering, leading to a decreased rate of physical weathering. The relatively unchanged annual precipitation may maintain a largely stable vegetation cover. Consequently, it might be expected that the valley has tended to be in an incision phase over the last half-century, and if the climatic trends shown in Fig. 11 were to continue, GLP would experience a decreased sediment supply. Under such a scenario, the likelihood of debris flows/debris-charged floods influencing the populations who live on alluvial fans

would decrease in the future. However, this does not exclude shorter term phases of aggradation brought about by debris flows, and is contingent upon the same patterns of climate change continuing into the future. Moreover, because the F4, F3 and F2 alluvial fans are occupied by people, human activities may influence the present incision trend of the valley. Associated activities include logging and rock mining in the limestone headwaters, which can lead to an increase of sediment supply. Nevertheless, the general trend of valley incision may be applicable to many other intermediate-sized valleys in the region because many of these valleys have also developed wide and deeply incised channels, indicating an active incision period at present. Continued incision would suggest that residents living on alluvial fans are less likely to be impacted directly by any debris flow/debris-charged flood events.

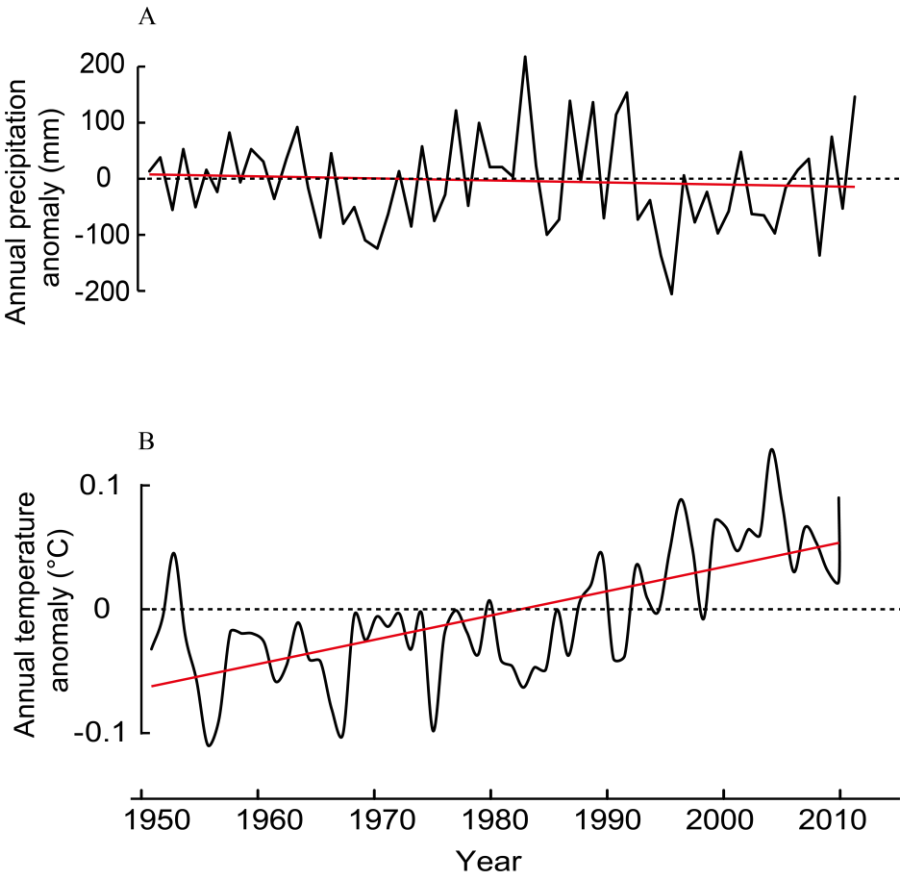

692

693 Fig. 11. Annual precipitation (A) and temperature (B) anomalies between 1950
694 and 2012 from the Wudu meteorological station, ~ 20 km from GLP. Red lines
695 are the overall trend based on linear regression.

696

697 **6. Conclusion**

698 This paper reconstructs the aggradation/incision history of GLP valley by dating
699 fine silt-sized quartz from alluvial terraces/fans and loess deposits using OSL
700 dating. By examining the temporal correlations between the observed phases of
701 aggradation and incision and regional climate records, we find that the warm and

wet mid-Holocene was dominated by rapid valley incision while the cold period from MIS 4 to the early Holocene and the short dry periods between 3.3 and 0.6 ka were dominated by aggradation in GLP. Cold conditions are considered to have enhanced frost shattering, while dry conditions led to deteriorated vegetation cover. Both effects led to an increase of sediment supply in the limestone headwaters. These sediments were transported by infrequent flood discharges, forming alluvial fan/terrace deposits. Phases of rapid incision during warm and humid periods are attributed to decreased sediment supply due to recovered vegetation cover and increased frequency of flooding.

We also examined the temperature and precipitation records in the study area between 1950 and 2012. These modern climatic records indicate a measurable warming trend with generally stable precipitation over the last 62 yr. This climatic trend is interpreted as indicating a decreased sediment supply resulting from impeded frost shattering and a stable vegetation cover over recent decades. Consequently, we conclude that the valley is likely to experience further incision if this trend continues.

Acknowledgments

This research was supported by the National Key Research and Development

722 Program of China (Project No. 2017YFC1501005), the National Natural Science
723 Foundation of China (Grant No. 41661144046), the Key Technology Research
724 and Development Program of the Ministry of Gansu Province, China (Grant No.
725 1604FKCA098) and the National Key Technology R&D Program, China (No. 309
726 2011BAK12B06). The authors thank Dr. Peng Guo, Dr. Guan Chen, Dr. Muqi
727 Xiong, Mr. Feng Qing, Mr. Zhijie Cui, and Mr. Yan Zhao for their help in the field.
728 Yajun Li thanks the Chinese Scholarship Council for supporting his living cost in
729 the UK. Simon Armitage's contribution to this work was partly supported by the
730 Research Council of Norway, through its Centres of Excellence funding scheme,
731 SFF Centre for Early Sapiens Behaviour (SapienCE), project number 262618.
732 The manuscript was greatly improved by reviews from two anonymous
733 reviewers and Professor Scott Lecce.

734

735 **References**

736 Adamiec, G., Aitken, M.J., 1998. Dose-rate conversion factors: update. Ancient
737 TL 16, 37-50.

738

739 Al-Farraj, A., Harvey, A.M., 2000. Desert pavement characteristics on wadi
740 terrace and alluvial fan surfaces: Wadi Al-Bih, UAE and Oman. Geomorphology
741 35, 279-297.

742

743 Al-Farraj, A., Harvey, A.M., 2005. Morphometry and depositional style of Late
744 Pleistocene alluvial fans: Wadi Al-Bih, northern UAE and Oman. Geological
745 Society, London, Special Publications 251, 85-94.
746
747 An, C., Feng, Z., Tang, L., 2003. Evidence of a humid mid-Holocene in the
748 western part of Chinese Loess Plateau. Chinese Science Bulletin 48, 2472-2479.
749
750 Anderson, R.S., 1998. Near-surface thermal profiles in alpine bedrock:
751 Implications for the frost weathering of rock. Arctic and Alpine Research 362-
752 372.
753
754 Armitage, S.J., Bailey, R.M., 2005. The measurement dependence of laboratory
755 beta dose rates on sample grain size. Radiation Measurements 39, 123 - 127.
756
757 Bell, W., 1980. Alpha dose attenuation in quartz grains for thermoluminescence
758 dating. Ancient TL 12, 8.
759
760 Blair, T.C., McPherson, J.G., 1994. Alluvial fan processes and forms,
761 Geomorphology of Desert Environments. Springer, pp. 354-402.
762
763 Bøtter-Jensen, L., Andersen, C., Duller, G.A., Murray, A.S., 2003. Developments
764 in radiation, stimulation and observation facilities in luminescence

765 measurements. Radiation Measurements 37, 535-541.

766

767 Bull, W.B., 1991. Geomorphic responses to climatic change.Oxford University
768 Press, Oxford.

769

770 Bull, W.B., 2000. Correlation of fluvial aggradation events to times of global
771 climate change. Quaternary Geochronology: Methods and Applications, 456-
772 464.

773

774 Buylaert, J.-P., Vandenberghe, D., Murray, A., Huot, S., De Corte, F., Van den
775 Haute, P., 2007. Luminescence dating of old (> 70ka) Chinese loess: a
776 comparison of single-aliquot OSL and IRSL techniques. Quaternary
777 Geochronology 2, 9-14.

778

779 Chapot, M., Roberts, H., Duller, G., Lai, Z., 2012. A comparison of natural-and
780 laboratory-generated dose response curves for quartz optically stimulated
781 luminescence signals from Chinese Loess. Radiation Measurements 47, 1045-
782 1052.

783

784 Chen, F., Xu, Q., Chen, J., Birks, H.J.B., Liu, J., Zhang, S., Jin, L., An, C., Telford,
785 R.J., Cao, X., 2015. East Asian summer monsoon precipitation variability since
786 the last deglaciation. Scientific Reports 5, 11186.

787 Chen, J., Dai, F., Yao, X., 2008. Holocene debris-flow deposits and their
788 implications on the climate in the upper Jinsha River valley, China.
789 Geomorphology 93, 493-500.

790

791 Clark, M.K., Royden, L.H., 2000. Topographic ooze: Building the eastern margin
792 of Tibet by lower crustal flow. Geology 28, 703-706.

793

794 Coulthard, T., Lewin, J., Macklin, M., 2005. Modelling differential catchment
795 response to environmental change. Geomorphology 69, 222-241.

796

797 Fan, M., 2006. The analysis of the formation of rainstorm and mud-rock flow and
798 landslide in Longnan. Nanjing University of information Science & Technology,
799 Nanjing.

800

801 Feng, Z.-D., Tang, L., Wang, H., Ma, Y., Liu, K.-b., 2006. Holocene vegetation
802 variations and the associated environmental changes in the western part of the
803 Chinese Loess Plateau. Palaeogeography, Palaeoclimatology, Palaeoecology
804 241, 440-456.

805

806 Fowler, A., Hennessy, K., 1995. Potential impacts of global warming on the
807 frequency and magnitude of heavy precipitation. Natural Hazards 11, 283-303.

Galbraith, R., Roberts, R.G., 2012. Statistical aspects of equivalent dose and error calculation and display in OSL dating: an overview and some recommendations. Quaternary Geochronology 11, 1-27.

Hales, T., Roering, J.J., 2007. Climatic controls on frost cracking and implications for the evolution of bedrock landscapes. Journal of Geophysical Research: Earth Surface 112.

Harvey, A.M., 1997. The role of alluvial fans in arid zone fluvial systems. Arid Zone Geomorphology: Processes, Form and Change in Drylands, pp. 231-259.

Harvey, A.M., 2002. The role of base-level change in the dissection of alluvial fans: case studies from southeast Spain and Nevada. Geomorphology 45, 67-87.

Harvey, A.M., 2011. Dryland alluvial fans. Arid Zone Geomorphology: Process, Form and Change in Drylands, Third Edition, pp. 333-371.

Harvey, A.M., 2012. The coupling status of alluvial fans and debris cones: a review and synthesis. Earth Surface Processes and Landforms 37, 64-76.

Harvey, A.M., Renwick, W., 1987. Holocene alluvial fan and terrace formation in the Bowland Fells, northwest England. Earth Surface Processes and Landforms 12, 249-257.

Harvey, A.M., Wigand, P.E., Wells, S.G., 1999. Response of alluvial fan systems to the late Pleistocene to Holocene climatic transition: contrasts between the margins of pluvial Lakes Lahontan and Mojave, Nevada and California, USA. Catena 36, 255-281.

Harvey, A.M., Stokes, M., Mather, A., Whitfield, E., 2016. Spatial characteristics of the Pliocene to modern alluvial fan successions in the uplifted sedimentary basins of Almería, SE Spain: review and regional synthesis. Geological Society, London, Special Publications 440, SP440. 445.

He, Z., Zhang, X., Qiao, Y., Bao, S., Lu, C., He, X., 2015. Formation of the Yalong downstream terraces in the SE Tibetan Plateau and its implication for the uplift of the plateau. Acta Geologica Sinica (English Edition) 89, 542-560.

Herman, F., Champagnac, J.D., 2016. Plio-Pleistocene increase of erosion rates in mountain belts in response to climate change. Terra Nova 28, 2-10.

Hu, Z.Z., Yang, S., Wu, R., 2003. Long-term climate variations in China and global warming signals. Journal of Geophysical Research: Atmospheres 108.

852

853 Huang, W.L., Yang, X.P., Li, A., Thompson, J.A., Zhang, L., 2014. Climatically
854 controlled formation of river terraces in a tectonically active region along the
855 southern piedmont of the Tian Shan, NW China. Geomorphology 220, 15-29.

856

857 Jakob, M., 2005. Debris-flow hazard analysis. Debris-flow hazards and related
858 phenomena, 411-443.

859

860 Johnson, K.R., Ingram, B.L., Sharp, W.D., Zhang, P., 2006. East Asian summer
861 monsoon variability during Marine Isotope Stage 5 based on speleothem δ ^{18}O
862 records from Wanxiang Cave, central China. Palaeogeography,
863 Palaeoclimatology, Palaeoecology 236, 5-19.

864

865 Juyal, N., Sundriyal, Y., Rana, N., Chaudhary, S., Singhvi, A.K., 2010. Late
866 Quaternary fluvial aggradation and incision in the monsoon-dominated
867 Alaknanda valley, Central Himalaya, Uttrakhand, India. Journal of Quaternary
868 Science 25, 1-13.

869

870 Kar, R., Chakraborty, T., Chakraborty, C., Ghosh, P., Tyagi, A.K., Singhvi, A.K.,
871 2014. Morpho-sedimentary characteristics of the Quaternary Matiali fan and
872 associated river terraces, Jalpaiguri, India: Implications for climatic controls.
873 Geomorphology 227, 137-152.

Kirby, E., Reiners, P.W., Krol, M.A., Whipple, K.X., Hodges, K.V., Farley, K.A., Tang, W., Chen, Z., 2002. Late Cenozoic evolution of the eastern margin of the Tibetan Plateau: inferences from 40Ar/39Ar and (U-Th)/He thermochronology. Tectonics 21, 1-1-1-20.

Knox, J.C., 1993. Large increases in flood magnitude in response to modest changes in climate. Nature 361, 430-432.

Kumar, R., Suresh, N., Sangode, S.J., Kumaravel, V., 2007. Evolution of the Quaternary alluvial fan system in the Himalayan foreland basin: implications for tectonic and climatic decoupling. Quaternary International 159, 6-20.

Lai, Z.P., 2006. Testing the use of an OSL standardised growth curve (SGC) for determination on quartz from the Chinese Loess Plateau. Radiation Measurements 41, 9-16.

Lai, Z.P., 2010. Chronology and the upper dating limit for loess samples from Luochuan section in the Chinese Loess Plateau using quartz OSL SAR protocol. Journal of Asian Earth Sciences 37, 176-185.

Lai, Z.P., Brückner, H., Zöller, L., Fülling, A., 2007. Existence of a common

growth curve for silt-sized quartz OSL of loess from different continents. Radiation Measurements 42, 1432-1440.

Li, J., Feng, Z., Tang, L., 1988. Late Quaternary monsoon patterns on the Loess Plateau of China. Earth Surface Processes and Landforms 13, 125-135.

Li, Y., 1994. On obduction nappe structure of Bailongjinag Region. Acta Geologica Gansu 3, 41-49.

Liang, X., Chen, H., Tang, H., 2010. Studies on debris flow development properties in Quaternary on the eastern edge of Qinghai-Tibet Plateau. Journal of Chongqing Jiaotong University (Natrual Science) 29, 978-983.

Lisiecki, L.E., Raymo, M.E., 2005. A Pliocene‐Pleistocene stack of 57 globally distributed benthic δ18O records. Paleoceanography 20.

Liu, J., Chen, J., Zhang, X., Li, Y., Rao, Z., Chen, F., 2015. Holocene East Asian summer monsoon records in northern China and their inconsistency with Chinese stalagmite δ 18 O records. Earth-Science Reviews 148, 194-208.

Lu, H., Burbank, D.W., Li, Y., 2010. Alluvial sequence in the north piedmont of the Chinese Tian Shan over the past 550kyr and its relationship to climate

change. Palaeogeography, Palaeoclimatology, Palaeoecology 285, 343-353.

Lu, H., Yi, S., Liu, Z., Mason, J.A., Jiang, D., Cheng, J., Stevens, T., Xu, Z., Zhang, E., Jin, L., 2013. Variation of East Asian monsoon precipitation during the past 21 ky and potential CO2 forcing. Geology 41, 1023-1026.

Maher, B.A., Thompson, R., 2012. Oxygen isotopes from Chinese caves: records not of monsoon rainfall but of circulation regime. Journal of Quaternary Science 27, 615-624.

Mather, A.E., Stokes, M., 2017. Bedrock structural control on catchment-scale connectivity and alluvial fan processes, High Atlas Mountains, Morocco. Geological Society, London, Special Publications 440, SP440. 415.

Mather, A.E., Stokes, M., Whitfield, E., 2017. River terraces and alluvial fans: the case for an integrated Quaternary fluvial archive. Quaternary Science Reviews 166, 74-90.

McDonald, E.V., McFadden, L.D., Wells, S.G., 2003. Regional response of alluvial fans to the Pleistocene-Holocene climatic transition, Mojave Desert, California. Special Papers-Geological Society of America, 189-206.

940 Mejdahl, V., 1979. Thermoluminescence dating: beta-dose attenuation in quartz
941 grains. Archaeometry 21, 61-72.
942
943 Miller, D.M., Schmidt, K.M., Mahan, S.A., McGeehin, J.P., Owen, L.A., Barron,
944 J.A., Lehmkuhl, F., Löhrer, R., 2010. Holocene landscape response to
945 seasonality of storms in the Mojave Desert. Quaternary International 215, 45-61.
946
947 Murray, A.S., Wintle, A.G., 2000. Luminescence dating of quartz using an
948 improved single-aliquot regenerative-dose protocol. Radiation measurements
949 32, 57-73.
950
951 Ouimet, W.B., Whipple, K.X., Royden, L.H., Sun, Z., Chen, Z., 2007. The
952 influence of large landslides on river incision in a transient landscape: eastern
953 margin of the Tibetan Plateau (Sichuan, China). Geological Society of America
954 Bulletin 119, 1462-1476.
955
956 Owen, L.A., Clemmens, S.J., Finkel, R.C., Gray, H., 2014. Late Quaternary
957 alluvial fans at the eastern end of the San Bernardino Mountains, Southern
958 California. Quaternary Science Reviews 87, 114-134.
959
960 Owen, L.A., Windley, B., Cunningham, W., Badamgarov, J., Dorjnamjaa, D.,
961 1997. Quaternary alluvial fans in the Gobi of southern Mongolia: evidence for

neotectonics and climate change. Journal of Quaternary Science 12, 239-252.

Phillips, J., 2006. Evolutionary geomorphology: thresholds and nonlinearity in landform response to environmental change.Hydrology and Earth System Sciences 10, 731-742.

Pope, R.J., Wilkinson, K.N., 2005. Reconciling the roles of climate and tectonics in Late Quaternary fan development on the Spartan piedmont, Greece. Geological Society, London, Special Publications 251, 133-152.

Prescott, J.R., Hutton, J.T., 1994. Cosmic ray contributions to dose rates for luminescence and ESR dating: large depths and long-term time variations. Radiation Measurements 23, 497-500.

Railsback, L.B., Xiao, H., Liang, F., Akers, P.D., Brook, G.A., Dennis, W.M., Lanier, T.E., Tan, M., Cheng, H., Edwards, R.L., 2014. A stalagmite record of abrupt climate change and possible Westerlies-derived atmospheric precipitation during the Penultimate Glacial Maximum in northern China. Palaeogeography, Palaeoclimatology, Palaeoecology 393, 30-44.

Rees-Jones, J., 1995. Optical dating of young sediments using fine-grain quartz. Ancient TL 13, 9-14.

Ritter, J.B., Miller, J.R., Enzel, Y., Wells, S.G., 1995. Reconciling the roles of tectonism and climate in Quaternary alluvial fan evolution. Geology 23, 245-248.

Santangelo, N., Daunis-i-Estadella, J., Di Crescenzo, G., Di Donato, V., Faillace, P., Martín-Fernández, J., Romano, P., Santo, A., Scorpio, V., 2012. Topographic predictors of susceptibility to alluvial fan flooding, Southern Apennines. Earth Surface Processes and Landforms 37, 803-817.

Schumm, S.A., 1979. Geomorphic thresholds: the concept and its applications. Transactions of the Institute of British Geographers, 485-515.

Sohn, M., Mahan, S., Knott, J., Bowman, D., 2007. Luminescence ages for alluvial-fan deposits in Southern Death Valley: implications for climate-driven sedimentation along a tectonically active mountain front. Quaternary International 166, 49-60.

Spelz, R.M., Fletcher, J.M., Owen, L.A., Caffee, M.W., 2008. Quaternary alluvial-fan development, climate and morphologic dating of fault scarps in Laguna Salada, Baja California, Mexico. Geomorphology 102, 578-594.

Stevens, T., Lu, H., Thomas, D.S., Armitage, S.J., 2008. Optical dating of abrupt

shifts in the late Pleistocene East Asian monsoon. Geology 36, 415-418.

Stokes, M., Mather, A.E., 2015. Controls on modern tributary-junction alluvial fan occurrence and morphology: High Atlas Mountains, Morocco. Geomorphology 248, 344-362.

Suresh, N., Bagati, T.N., Kumar, R., Thakur, V.C., 2007. Evolution of Quaternary alluvial fans and terraces in the intramontane Pinjaur Dun, Sub-Himalaya, NW India: interaction between tectonics and climate change. Sedimentology 54, 809-833.

Tan, M., 2014. Circulation effect: response of precipitation $\delta^{18}O$ to the ENSO cycle in monsoon regions of China. Climate Dynamics 42, 1067-1077.

Tang, C., Rengers, N., van Asch, T.W., Yang, Y., Wang, G., Luino, F., 2011. Triggering conditions and depositional characteristics of a disastrous debris flow event in Zhouqu city, Gansu Province, northwestern China. Natural Hazards & Earth System Sciences 11, 2903-2912.

Walder, J., Hallet, B., 1985. A theoretical model of the fracture of rock during freezing. Geological Society of America Bulletin 96, 336-346.

Wang, A., Smith, J.A., Wang, G., Zhang, K., Xiang, S., Liu, D., 2009. Late Quaternary river terrace sequences in the eastern Kunlun Range, northern Tibet: A combined record of climatic change and surface uplift. Journal of Asian Earth Sciences 34, 532-543.

Wang, H., Chen, J., Zhang, X., Chen, F., 2014. Palaeosol development in the Chinese Loess Plateau as an indicator of the strength of the East Asian summer monsoon: Evidence for a mid-Holocene maximum. Quaternary International 334, 155-164.

Wang, P.X., Wang, B., Cheng, H., Fasullo, J., Guo, Z., Kiefer, T., Liu, Z., 2017. The global monsoon across time scales: Mechanisms and outstanding issues. Earth-Science Reviews 174, 84-121.

Wang, Y.J., Cheng, H., Edwards, R.L., Kong, X., Shao, X., Chen, S., Wu, J., Jiang, X., Wang, X., An, Z., 2008. Millennial-and orbital-scale changes in the East Asian monsoon over the past 224,000 years. Nature 451, 1090-1093.

Wang, Y.J., Cheng, H., Edwards, R.L., An, Z., Wu, J., Shen, C.-C., Dorale, J.A., 2001. A high-resolution absolute-dated late Pleistocene monsoon record from Hulu Cave, China. Science 294, 2345-2348.

Wells, S.G., Harvey, A.M., 1987. Sedimentologic and geomorphic variations in storm-generated alluvial fans, Howgill Fells, northwest England. Geological Society of America Bulletin 98, 182-198.

Welsh, A., Davies, T., 2011. Identification of alluvial fans susceptible to debris-flow hazards. Landslides 8, 183-194.

Wilford, D., Sakals, M., Innes, J., Sidle, R., Bergerud, W., 2004. Recognition of debris flow, debris flood and flood hazard through watershed morphometrics. Landslides 1, 61-66.

Wintle, A.G., 2008. Luminescence dating: where it has been and where it is going. Boreas 37, 471 - 482.

Xiong, M., Meng, X., Wang, S., Guo, P., Li, Y., Chen, G., Qing, F., Cui, Z., Zhao, Y., 2016. Effectiveness of debris flow mitigation strategies in mountainous regions. Progress in Physical Geography, 0309133316655304.

Yang, H., Johnson, K., Griffiths, M., Yoshimura, K., 2016. Interannual controls on oxygen isotope variability in Asian monsoon precipitation and implications for paleoclimate reconstructions. Journal of Geophysical Research: Atmospheres 121, 8410-8428.

1072

1073 Zhang, M., Li, Z., Wang, G., 2011. The geological hazard characteristics and

1074 exploration ideas of the Bailong River Basin. Northeastern Geology 44, 1-9.

1075

1076